Themed Issue





Themed Issue on Hypoxia and Living Resources in the Gulf of Mexico

Using a coupled ecosystem modeling approach to evaluate effects of reductions in nutrients and hypoxia on living marine resources

Kim de Mutsert^{1,*©}, Sara Marriott¹, Joe Buszowski², Arnaud Laurent³, and Katja Fennel³

School of Ocean Science and Engineering, Division of Coastal Sciences, The University of Southern Mississippi, Ocean Springs, Mississippi, USA

> ²Ecopath International Initiative, Barcelona, Spain ³Department of Oceanography, Dalhousie University, Halifax, Nova Scotia, Canada

> > *Corresponding author: Kim de Mutsert. Email: kim.demutsert@usm.edu.

ABSTRACT

Objective: The objective of this study was to evaluate effects of planned reductions in hypoxia on fish and fisheries in the northern Gulf of Mexico. To specifically address goals established by the Hypoxia Task Force, a short-term goal of 20% reduction in nitrogen and phosphorus loading from the Mississippi River and long-term goals of 40% and 50% reductions in nitrogen and phosphorus loading (encompassing the goal of reducing the 5-year average hypoxic area size to 5,000 km²) were used as model scenarios.

Methods: An Ecospace model was co-produced representing the northern Gulf of Mexico food web, with 66 groups of fish, shellfish, and other marine organisms. Four species of high economic and/or ecological interest were the focus of this paper: Red Snapper Lutjanus campechanus, Gulf Menhaden Brevoortia patronus, Atlantic Croaker Micropogonias undulatus, and white shrimp Penaeus setiferus. The Ecospace model was linked to a calibrated physical-biological Regional Ocean Modeling System-based model that passed dissolved oxygen, phytoplankton, and temperature output of the simulation scenarios on to Ecospace. Novel spatial Monte Carlo simulations were used to determine the probability of the outcomes and calculate uncertainty ranges.

Results: Hypoxia affected all organisms to some extent, either by avoidance of hypoxic areas or by a decrease in biomass. Under simulated nutrient reduction scenarios, the biomass of some species increased (e.g., Gulf Menhaden and white shrimp), while the biomass of other species decreased (e.g., Red Snapper and Atlantic Croaker). Although hypoxia affected the spatial distribution of species biomass, the total biomass changes in response to the nutrient reduction scenarios for the most part did not exceed the uncertainty bounds of the scenario in which nutrients were not reduced.

Conclusions: Exploring reductions in nutrient loading from the Mississippi River and the subsequent reductions in hypoxia separately and together revealed that reducing hypoxia has a positive effect on living resources, while reducing nutrients has a negative effect. The small net effects were specific to each species due to species-specific hypoxia sensitivities and trophic interactions. Nutrient reductions affected the spatial distribution by increasing fisheries species biomass in areas closer to the coast. The output of this coupled modeling approach supports managers in assessing effects of planned nutrient reduction goals on ecosystem function, living resources, and fisheries landings.

KEYWORDS: Ecopath with Ecosim, Ecospace, fisheries species, Gulf of Mexico, hypoxia, nutrient reductions, spatial modeling

LAY SUMMARY

This study simulated effects of nutrient reduction goals in the Gulf of Mexico on fisheries species. Total biomass was not strongly affected by nutrient and hypoxia reductions, but distribution was. Our simulations showed that avoidance of the area that currently experiences summer hypoxia would be reduced.

INTRODUCTION

Ocean deoxygenation and hypoxia have become significant concerns in various marine ecosystems around the world, including the northern Gulf of Mexico. Hypoxia refers to an oxygen deficiency in aquatic environments, resulting in low oxygen concentrations (typically defined as less than 2 mg/L) that are inadequate to support most marine organisms. The Gulf of Mexico, known for its diverse marine life and thriving fisheries, has experienced a hypoxic zone over the past few decades (Rabalais & Turner, 2019). The northern Gulf of Mexico is particularly susceptible to hypoxia due to the confluence of several factors. The excessive nutrient runoff from agricultural activities and urbanization in the Mississippi River watershed is a major contributor to the formation of the hypoxic zone (Rabalais et al., 2001). These nutrients, primarily nitrogen (N) and phosphorus (P), enter the Gulf of Mexico and fuel the growth of phytoplankton, leading to algal blooms. As these algae die and decompose, oxygen in the water is consumed, exacerbating the depletion of dissolved oxygen (DO) levels. Over time, the hypoxic zone in the northern Gulf of Mexico has expanded both in size and duration. The zone has increased from smaller than 10,000 km2 in the 1980s to as large as 23,000 km² in recent years (Rabalais & Turner, 2019). Hypoxia is known to have effects on fish and shellfish (Kim et al., 2023). Fish species that cannot tolerate low-oxygen conditions either relocate to areas with higher oxygen concentrations (avoidance) or suffer from mortality, physiological stress, and reduced reproductive success. The hypoxic zone acts as a barrier to fish movements, leading to habitat compression and decreased access to food and suitable breeding grounds. This can result in altered fish migration patterns and reduced population sizes, potentially affecting the overall productivity of Gulf of Mexico fisheries (Craig, 2012). The ecological disruption caused by hypoxia can have cascading effects on the entire marine food web, including the loss of commercially and recreationally valuable species and changes in species composition. A decline in fish populations and reduced catch potential would affect the economic viability of commercial and recreational fisheries in the northern Gulf of Mexico (Smith et al., 2017).

The Mississippi River/Gulf of Mexico Hypoxia Task Force (HTF), established in 1997, aims to investigate the causes and impacts of eutrophication in the Gulf of Mexico; coordinate efforts to minimize the size, severity, and duration of the hypoxic zone; and mitigate the effects of hypoxia (U.S. Environmental Protection Agency, 2025). Efforts to reduce hypoxia in the northern Gulf of Mexico include decreasing the nutrient load entering the Mississippi River in the Mississippi watershed. The Gulf of Mexico hypoxia action plan goals of the HTF are to reduce the 5-year running average size of the Gulf hypoxic zone to 5,000 km², with an interim goal of a 20% reduction in N and P (hereafter, "N&P") loading from the Mississippi–Atchafalaya River basin (U.S. Environmental Protection Agency, 2025).

The goal of our work is to evaluate the effects of Mississippi River nutrient load reductions in combination with resulting hypoxia mitigation on fish and fisheries using coupled spatially explicit ecosystem and water quality models and to develop a decision support tool that visualizes the output. Earlier research has shown that when reducing nutrient loading, there is a

trade-off between (1) having an environmental improvement that can increase fish and shellfish biomass because hypoxia is reduced and (2) having reduced primary productivity that can decrease fish and shellfish biomass productivity (Breitburg, 2002; De Mutsert et al., 2016).

To account for these opposing responses of fisheries species to nutrient reductions in simulations, an ecosystem approach was used that included the effects of nutrient reductions on phytoplankton and trophic interactions and the effects of hypoxia on foraging and movement of nekton species in an extensive food web. For this, we used the ecosystem modeling tool Ecospace, which is the spatial module of Ecopath with Ecosim that allows for the inclusion of these factors as well as fisheries (Christensen & Walters, 2024). The spatially explicit nature of Ecospace makes it a good tool for addressing spatial problems, such as the hypoxic zone in the northern Gulf of Mexico (De Mutsert et al., 2024), especially when the research questions pertain to what may happen if the size of the hypoxic zone is reduced.

To increase the application of the research, members of the HTF as well as environmental resource managers representing 11 regional institutions participated in an advisory panel during this project. The details of the co-production process and the development of the decision support tool that visualizes the results of this work can be found in Shaffer et al. (2023). The ultimate goal of this work is to help resource managers anticipate effects of the management actions to reduce nutrient loading from the Mississippi River on living marine resources in the northern Gulf of Mexico.

METHODS

An Ecospace model representing the food web was developed using Ecopath with Ecosim software (https://ecopath.org/) coupled to a published Regional Ocean Modeling System (ROMS)-based physical-biological model from which it received DO, salinity, temperature, and phytoplankton output (Fennel et al., 2011; Laurent & Fennel, 2014). Groups in the model include marine mammals, seabirds, turtles, fish, shellfish, zooplankton, benthic invertebrates, phytoplankton, and detritus. While the model simulates the food web represented by 66 groups, we focus on the following four species of ecological or economic interest: Atlantic Croaker Micropogonias undulatus, Gulf Menhaden Brevoortia patronus, Red Snapper Lutjanus campechanus, and white shrimp Penaeus setiferus. The coupled model was calibrated using existing conditions from 2000 to 2016, after which scenarios for short-term (~10 years) and long-term (~20 years) hypoxia reductions were explored. Earlier work with the ROMS model established that reducing the size of the hypoxic zone to 5,000 km² requires an N&P load reduction between 40% and 50% (Fennel & Laurent, 2018), so we decided to run four scenarios: no nutrient reduction (100% N&P), 20% N&P reduction (the interim goal), 40% N&P reduction, and 50% N&P reduction. We ran each scenario from 2000 to 2035. Novel spatial Monte Carlo simulations were performed to estimate the uncertainty of the predictions.

Model domain and research area

The model area represents the northern Gulf of Mexico off the coast of Louisiana in two dimensions, with 10,318 active 5-km²

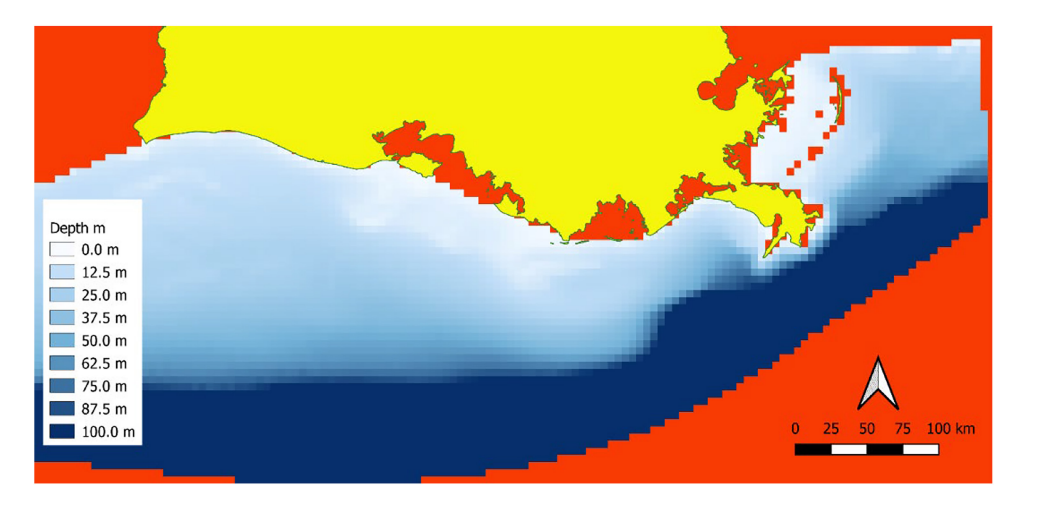


Figure 1. Ecospace model area, with active cells in the white-blue color range and excluded cells in orange. The state of Louisiana is overlaid in yellow as a geographical reference.

cells (Figure 1). This model domain encompasses the hypoxic zone in the northern Gulf of Mexico. The Ecospace model area matches the spatial extent of the physical–biological model to which it is linked.

The physical-biological model

The coupled physical-biological model linked to the Ecospace model has been used to investigate the mechanisms controlling hypoxia in the northern Gulf of Mexico (Fennel & Laurent, 2018; Fennel et al., 2011; Laurent & Fennel, 2014). Hypoxia mitigation strategies were assessed using nutrient reduction scenarios (Fennel & Laurent, 2018), some of which are used in the Ecospace model. The circulation model is implemented with ROMS (Haidvogel et al., 2008; Shchepetkin & McWilliams, 2005) to simulate water circulation patterns along the northern Gulf of Mexico shelf near the Mississippi and Atchafalaya River outflows (Hetland & DiMarco, 2008, 2012). Configured with 20 layers, the model has enhanced resolution near both the surface and the seabed. Spatial resolution ranges from approximately 20 km in the southwestern corner to nearly 1 km around the delta of the Mississippi River. Meteorological inputs were applied using 3-hourly wind data from the North American Regional Reanalysis data set (National Centers for Environmental Prediction; Mesinger et al., 2006) and climatological heat and freshwater fluxes at the surface (da Silva et al., 1994). Daily freshwater influxes from the Mississippi and Atchafalaya rivers were determined by the U.S. Army Corps of Engineers' estimates at Tarbert Landing and Simmesport, respectively. Nutrient, particulate organic matter (POM), and dissolved organic matter (DOM) loading was based on monthly nutrient flux estimations from the U.S. Geological Survey (Aulenbach et al., 2007).

The biogeochemical model includes the pelagic N-cycle model devised by Fennel et al. (2006, 2008, 2011). This model encompassed two forms of dissolved inorganic N, namely nitrate (NO_3) and ammonium (NH_4), as well as components such as phytoplankton, chlorophyll, zooplankton, and two pools of POM: one that remains suspended and sinks gradually and another representing rapidly sinking detritus. Expansions to the model encompassed dissolved inorganic P (DIP; Laurent

et al., 2012), river DOM (Yu et al., 2015), and DO (O2; Fennel et al., 2013). Phytoplankton growth was constrained by temperature, light availability, and nutrient levels. The degree of nutrient limitation was contingent on the most limiting nutrient—either dissolved inorganic N (indicative of N limitation) or DIP (indicating P limitation), as explained by Laurent et al. (2012). Phytoplankton and suspended detrital matter combine to form rapidly sinking detritus; this sinking POM instantaneously undergoes remineralization into ammonium and DIP at the sediment-water interface. While all P returns to the water column as DIP, a constant proportion of N is lost through sediment denitrification. A thorough description of the instant remineralization parameterization is provided by Fennel et al. (2013, 2006). Within the model framework, oxygen was generated during primary production, utilized through respiration both in the water column and in sediment, and exchanged with the atmosphere across the air-sea interface.

Oxygen consumption in the water column resulted from zooplankton respiration, POM and refractory DOM remineralization, and light-dependent nitrification. The instant remineralization parameterization inferred that oxygen was consumed in the sediment due to nitrification and aerobic remineralization only, adhering to a constant ratio between aerobic organic matter remineralization and denitrification—a ratio following the linear relationship between sediment oxygen consumption and denitrification outlined by Seitzinger and Giblin (1996). The model was calibrated with atmospheric conditions from the years 2000-2016 and was able to recreate DO and primary production accurately (Fennel & Laurent, 2018; Laurent & Fennel, 2014). The same 17-year simulation was repeated with reduced loads of total N&P as described by Fennel and Laurent (2018). The calibrated run without nutrient load reductions and the N&P load reductions of 20, 40, and 50% were used to create the scenarios in the Ecospace model.

The northern Gulf of Mexico ecosystem model

The ecosystem model is a spatial and temporal dynamic food web model developed in Ecopath with Ecosim software. This approach combines ecological data, mathematical modeling,

Table 1. Mass-balanced Ecopath parameters. The numbers in some of the model group names represent the age range of the group in months. Group names in bold italics indicate the groups that were calibrated in Ecosim. The superscripts on each of the values indicate the source of the information with references in the footnotes. An asterisk (*) denotes when a value was calculated by Ecopath. Abbreviations are as follows: P = production, B = biomass, Q = consumption, and EE = ecotrophic efficiency.

Group name	Reference species	Biomass (metric tons/km²)	P/B (per year)	Q/B (per year)	EE
Marine mammals	Common Bottlenose Dolphin Tursiops truncatus	0.069ª	0.02ª	11.97ª	0.144*
Tunas	Yellowfin Tuna Thunnus albacares	0.024^{q}	0.90 ^b	13.00 ^b	0.071*
Carangidae	Crevalle Jack Caranx hippos	0.012°	0.80°	3.30^{b}	0.091*
Birds	Brown Pelican Pelecanus occidentalis	0.011 ^s	0.25 ^s	35.00 ^s	0.017*
Juvenile Atlantic Cutlassfish	Atlantic Cutlassfish Trichiurus lepturus	0.002*	2.00 ^b	6.35*	0.577*
Adult Atlantic Cutlassfish	-	0.083^{q}	0.41^{b}	2.05^{b}	0.909*
Lizardfish	Inshore Lizardfish Synodus foetens	0.067^{q}	0.60^{b}	5.00^{b}	0.944*
Juvenile sharks	Bull Shark Carcharhinus leucas	0.001*	2.00^{b}	4.30*	0.814*
Adult sharks		0.020^{d}	0.58 ^d	1.49 ^b	0.554*
Juvenile King Mackerel	King Mackerel Scomberomorus cavalla	0.007*	1.40 ^b	9.80*	0.039*
Adult King Mackerel		0.118^{q}	0.90e	3.50e	0.022*
Juvenile Spanish Mackerel	Spanish Mackerel Scomberomorus maculatus	0.007*	2.00^{b}	19.43*	0.015*
Adult Spanish Mackerel		0.066^{f}	1.20 ^f	7.00^{f}	0.036*
0–3 seatrout	Spotted Seatrout Cynoscion nebulosus	0.000*	6.00 ^r	23.96*	0.546*
3–18 seatrout		0.016*	$1.40^{\rm r}$	4.11*	0.702*
18+ seatrout		0.147^{q}	$0.70^{\rm r}$	$1.60^{\rm r}$	0.443*
0-6 Red Snapper	Red Snapper Lutjanus campechanus	0.002*	3.00^{r}	22.11*	0.785*
6-24 Red Snapper		0.041^{g}	2.00^{r}	6.65 ^b	0.506*
24+ Red Snapper		1.149*	0.21^{g}	1.76*	0.267*
0-12 Serranidae	Yellowedge Grouper Hyporthodus flavolimbatus	0.001*	2.00^{r}	4.59*	0.622*
12-36 Serranidae		0.016*	$0.60^{\rm r}$	2.07*	0.231*
36+ Serranidae		0.041^{q}	0.45 ^r	1.30^{b}	0.106*
Other snappers	Gray Snapper Lutjanus griseus	0.035^{q}	1.30 ^h	13.70 ^b	0.263*
0-3 Red Drum	Red Drum Sciaenops ocellatus	0.000*	2.00^{r}	30.83*	0.034*
3-8 Red Drum		0.000*	3.50 ^r	11.16*	0.303*
8-18 Red Drum		0.002*	1.10^{r}	5.10*	0.344*
18–36 Red Drum		0.007*	$0.60^{\rm r}$	3.03*	0.533*
36+ Red Drum		0.078^{q}	0.15 ^r	1.86^{b}	0.769*
Juvenile rays and skates	Atlantic Stingray Hypanus sabinus	0.000*	2.00^{b}	4.49*	0.160*
Adult rays and skates		0.014^{9}	0.30 ^r	1.00 ^r	0.423*
Flounders	Southern Flounder Paralichthys lethostigma	0.046^{q}	0.42^{b}	7.00 ^b	0.178*
Atlantic Bumper	Atlantic Bumper Chloroscombrus chrysurus	0.113^{q}	1.20 ^r	9.00 ^b	0.964*
Scad	Rough Scad Trachurus lathami	0.0299	1.65 ^b	5.00 ^b	0.430*
Juvenile Atlantic Croaker	Atlantic Croaker Micropogonias undulatus	0.031*	2.00*	14.48*	0.783*
Adult Atlantic Croaker	77 11 10 01 1 1 1 1	0.709^{q}	0.70 ⁱ	4.72 ^b	0.714*
Catfish	Hardhead Catfish Ariopsis felis	0.0389	0.80 ^r	7.60°	0.899*
Juvenile Butterfish	Butterfish Peprilus triacanthus	0.001*	2.00 ^b	13.29*	0.392*
Adult Butterfish		0.1059	0.45 ^b	3.30 ^b	0.565*
Spot	Spot Leiostomus xanthurus	0.1314	0.70 ^b	12.00 ^r	0.825*
Squid	Northern Shortfin Squid Illex illecebrosus	0.0234	1.00 ^j	3.90 ^j	0.744*
Pinfish	Pinfish Lagodon rhomboides	0.025 ^q	2.00 ^b	5.00 ^b	0.664*
Porgies	Red Porgy Pagrus pagrus	0.253 ^q	2.52 ^k	8.00 ^b	0.584*
Anchovy	Bay Anchovy Anchoa mitchilli	0.010 ^q	2.53 ^r	14.00 ^r	0.792*
0-12 Gulf Menhaden	Gulf Menhaden Brevoortia patronus	3.403*	1.67 ¹	44.62*	0.078*
12-24 Gulf Menhaden		10.43*	1.42 ¹	22.40*	0.231*
24-36 Gulf Menhaden		5.207 ^l	2.37^{1}	15.70 ¹	0.603*
36+ Gulf Menhaden	Carlad Cardina III amenda i arrena (alaa ku arren	1.108*	2.08 ^l	12.30*	0.864*
Other clupeids	Scaled Sardine Harengula jaguana (also known as Harengula pensacola)	0.089 ^q	1.80 ^b	12.11 ^b	0.800*
Mullet	Striped Mullet Mugil cephalus	0.027 ^q	$0.80^{\rm r}$	8.00 ^r	0.854*
Sea turtles	Kemp's ridley sea turtle Lepidochelys kempii	0.019 ^q	0.11^{j}	6.76 ^j	0.005*
Small forage fish	Mummichog Fundulus heteroclitus	0.025 ^q	2.53 ^b	12.00 ^b	0.800*
Jellyfish	Moon jelly Aurelia aurita	0.013 ^q	22.00 ^j	67.00 ^j	0.205*
Blue crab	Blue crab Callinectes sapidus	0.038 ^q	2.76 ^m	8.50 ^r	0.416*
Juvenile brown shrimp	Brown shrimp Farfantepenaeus aztecus	0.001*	3.00 ^b	59.87*	0.276*
Adult brown shrimp	TATILITY of the state of the st	0.036 ⁿ	4.14 ⁿ	20.70 ⁿ	0.720*
Juvenile white shrimp Adult white shrimp	White shrimp Litopenaeus setiferus	0.016* 0.286°	3.00 ^b 5.24°	69.49* 26.20°	0.307* 0.461*

(Continued)

Table 1 continued.

	D. C.	Biomass (metric	P/B (per	Q/B (per	
Group name	Reference species	tons/km ²)	year)	year)	EE
Juvenile pink shrimp	Pink shrimp Farfantepenaeus duorarum	0.001*	3.00 ^b	56.09*	0.256*
Adult pink shrimp		0.027^{p}	3.74 ^p	18.70 ^p	0.929*
Other shrimp	Atlantic seabob Xiphopenaeus kroyeri	0.035^{q}	2.40^{r}	19.20^{r}	0.852*
Benthic crabs	Atlantic mud crab Panopeus herbstii	0.873 ^q	2.00^{r}	7.00^{r}	0.850*
Benthic invertebrates	Mantis shrimp Squilla empusa	4.060 ^q	4.50 ^r	22.00^{r}	0.850*
Zooplankton	Copepods Acartia spp.	7.642^{r}	$36.00^{\rm r}$	$89.00^{\rm r}$	0.280*
Benthic algae/weeds	Rhodophyta	29.78^{r}	25.00^{r}		0.017*
Phytoplankton	Diatoma	$25.00^{\rm r}$	182.13^{r}		0.244*
Detritus		100.0 ^r			0.014*

^aNational Marine Fisheries Service Office of Science and Technology (2017).

kSEDAR (2012).

¹SEDAR (2013c).

^mGulf Data, Assessment, and Review (2013).

ⁿHart (2015a).

°Hart (2015b).

PHart (2015c).

^qSoutheast Area Monitoring and Assessment Program survey data.

^sGeers et al. (2016).

and spatial representation to create a comprehensive model of the marine ecosystem. The model is an update from an earlier developed Ecospace model of the northern Gulf of Mexico (De Mutsert et al., 2016). Updates were mostly based on suggestions provided during a co-production workshop (described by Shaffer et al., 2023). Changes include increasing the number of groups in the model (from 60 to 66); using stock assessment data (for species with this information available) in addition to monitoring data and landings data to inform the model; updating the diet matrix based on diet data from a field study within the model area (Glaspie et al., 2019) and a diet meta-analysis of published literature (Sagarese et al., 2017); and having the base model represent the year 2000 (based on data from the period 1995-2000), which is the start of the physical-biological model simulations. During model development, an Ecopath model was first constructed, which represents a balanced snapshot of the northern Gulf of Mexico food web consisting of 66 groups that represent different species (with most split into two or more life stages) and functional groups within the ecosystem (Table 1; Figure 2). Each group is defined by its ecological characteristics, such as diet composition, biomass, production, and consumption rates. Relevant ecological data were gathered from fisheries surveys (Southeast Area Monitoring and Assessment Program [SEAMAP]; seamap.org), scientific databases (FishBase [fishbase.org] and SeaLifeBase [sealifebase. org]), stock assessment of fisheries resources, and published literature. The initial biomass (metric tons/km²) was based on SEAMAP survey data collected from 1995 to 2000 or stock assessments for fisheries resources (see Table 1 for sources of biomass and other Ecopath parameters). For SEAMAP survey

data, the area sampled was calculated by first converting the start and end points for each tow to a towing distance:

$$\begin{aligned} & distance \, towed \big(NM\big) \\ &= 60 \sqrt{(lat_{start} - lat_{end})^2 + (long_{start} - long_{end})^2 \times cos\theta^2} \,, \end{aligned} \tag{1}$$

where NM is nautical miles, lat is latitude, long is longitude, and θ represents the towing angle in radians, calculated as $\theta = 0.5(lat_{start} + lat_{end}) \times (\pi/180)$. The towing distance was used to determine the area sampled by multiplying by the tow width (0.012192 km) and converting from NM to trawl area sampled in square kilometers:

trawl area sampled_{SEAMAP}
$$\left(km^{2}\right)$$

= 1.852 × $\left[distance towed(NM)\right]$ × 0.012192.

The catch (metric tons) per unit effort for each species was divided by this sampling area. Finally, a 17% correction factor was used to correct for gear inefficiency of the trawl (Rozas & Minello, 1997). Fishery fleets were defined in the model as well, representing the most relevant fisheries in the northern Gulf of Mexico based on biomass or value. Fleets included in the model were shrimp trawls, menhaden purse seines, recreational anglers, a commercial fleet targeting the snapper-grouper complex, and a commercial fleet targeting other finfish. Initial landings were based on National Oceanic and Atmospheric Administration (NOAA) landings survey data from the years 1995-2000 and recreational landings estimates from

^bFishBase (www.fishbase.org).

^cSoutheast Data, Assessment, and Review (SEDAR), 2016a.

dSEDAR (2013a).

eSEDAR (2004).

fSEDAR (2013b)

gSEDAR (2015).

hSEDAR (2016b). SEDAR (2010).

^jSeaLifeBase (www.sealifebase.org).

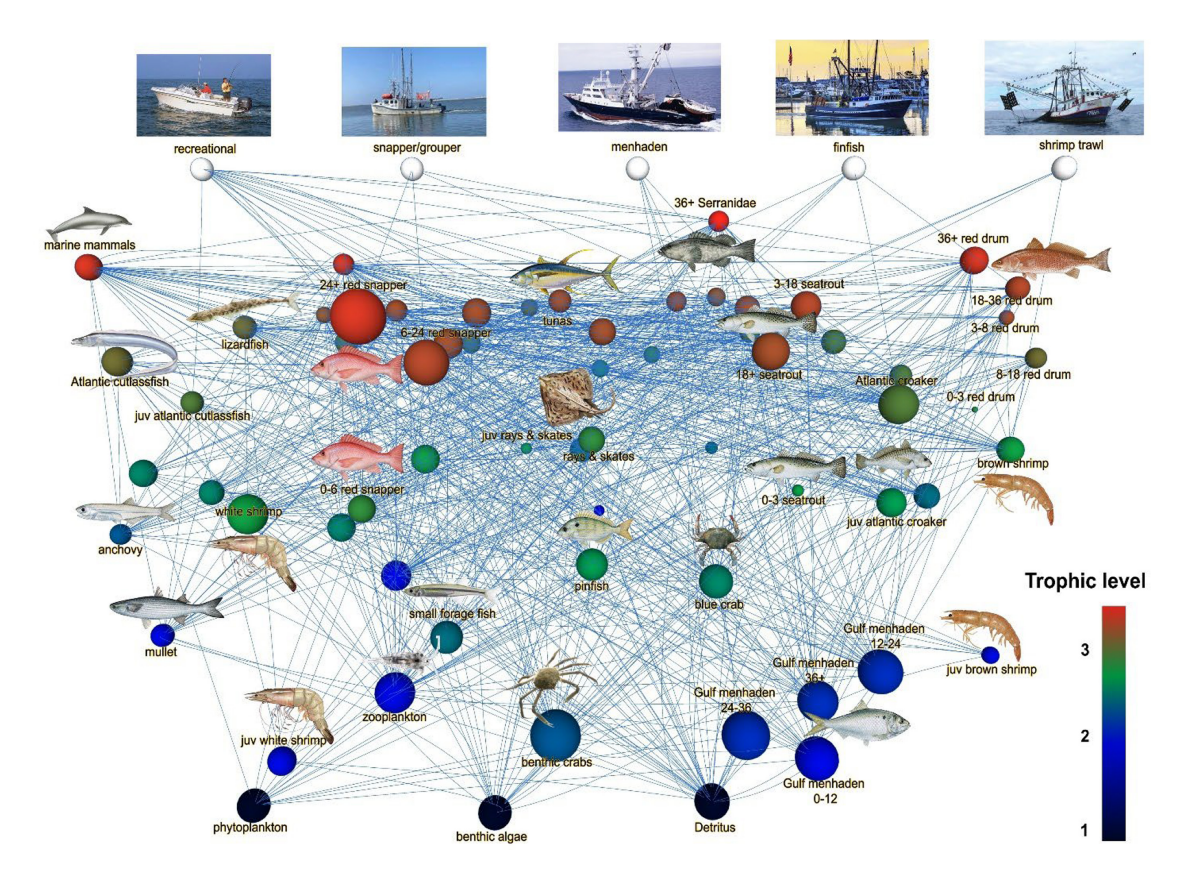


Figure 2. Balanced Ecopath model. Trophic interactions and fishing are indicated with connected lines. The color and vertical position of the nodes indicate the trophic level of the groups; the size of the nodes indicates the size of the biomass pool. The numbers in some of the model group names represent the age range of the group in months. Abbreviation is as follows: juv = juvenile.

the National Marine Fisheries Service's Marine Recreational Information Program (National Marine Fisheries Service, 2018). All data were downloaded in 2018.

The Ecopath model was balanced using Ecopath's first master equation (Christensen & Walters, 2004):

$$(P_i/B_i) \times B_i \times EE_i$$

$$-\sum_{(j=1)}^{n} B_j \times \left(\frac{Q_j}{B_i}\right) \times DC_{ji} - Y_i - E_i - BA_i = 0,$$
(3)

where (P_i/B_i) is the production-to-biomass ratio of model group i; B_i and B_j are the biomasses of the prey (group i) and the predators (group j), respectively; EE_i is the ecotrophic efficiency of group i; (Q_j/B_j) is the consumption-to-biomass ratio of group j; DC_{ji} is the fraction of group i in the diet of group j; Y_i is the catch rate of the fisheries for group i; E_i is the net migration rate for group i; and BA_i is the biomass accumulation for group i.

The model was calibrated by fitting the simulated outputs to observed data of biomass and landings in Ecosim. This iterative process involves adjusting vulnerability exchange rate parameter values and model structure to improve the model's fit to the real-world ecosystem. In Ecosim, prey biomass is partitioned into vulnerable and invulnerable components representing ecological or behavioral processes that restrict the rate at which prey become susceptible to predation (Walters & Martell, 2004). The

exchange rate between these components is called the vulnerability exchange rate, which regulates prey availability to predators and influences the extent to which fluctuations in predator biomass affect predation mortality. The SEAMAP surveys, NOAA fisheries landings, and stock assessment data from the period 2000-2016 were used to calibrate biomass, landings, and (in some cases) fishing mortality for all groups with this information available. Biomass from SEAMAP data was obtained in the same way as was explained for Ecopath, and the source of the biomass of each model group (SEAMAP surveys or stock assessment) was the same for Ecopath start biomass and Ecosim time series, as indicated in Table 1. Our calibration process followed the best practice demonstrated by Heymans et al. (2016) to estimate the vulnerability exchange rate parameters by calibrating model predictions to observed time series data and to base the decision of the best fit on both the sum of squares and Akaike's information criterion. We followed the approach described by Chagaris et al. (2020) to iteratively estimate the K-1 (where K is the number of time series fitted) most sensitive vulnerability exchange rates, but we followed the Bentley et al. (2021) approach of combining searches for predator vulnerability exchange rates and predator-prey vulnerability exchange rates. Finally, we constrained how much predation mortality by a given predator could increase relative to a prey's total natural mortality by calculating caps as introduced by Chagaris et al. (2020). Using this combination of approaches, our calibration process aligned with recently published calibration recommendations (Bentley et al., 2024). Thirty-four groups

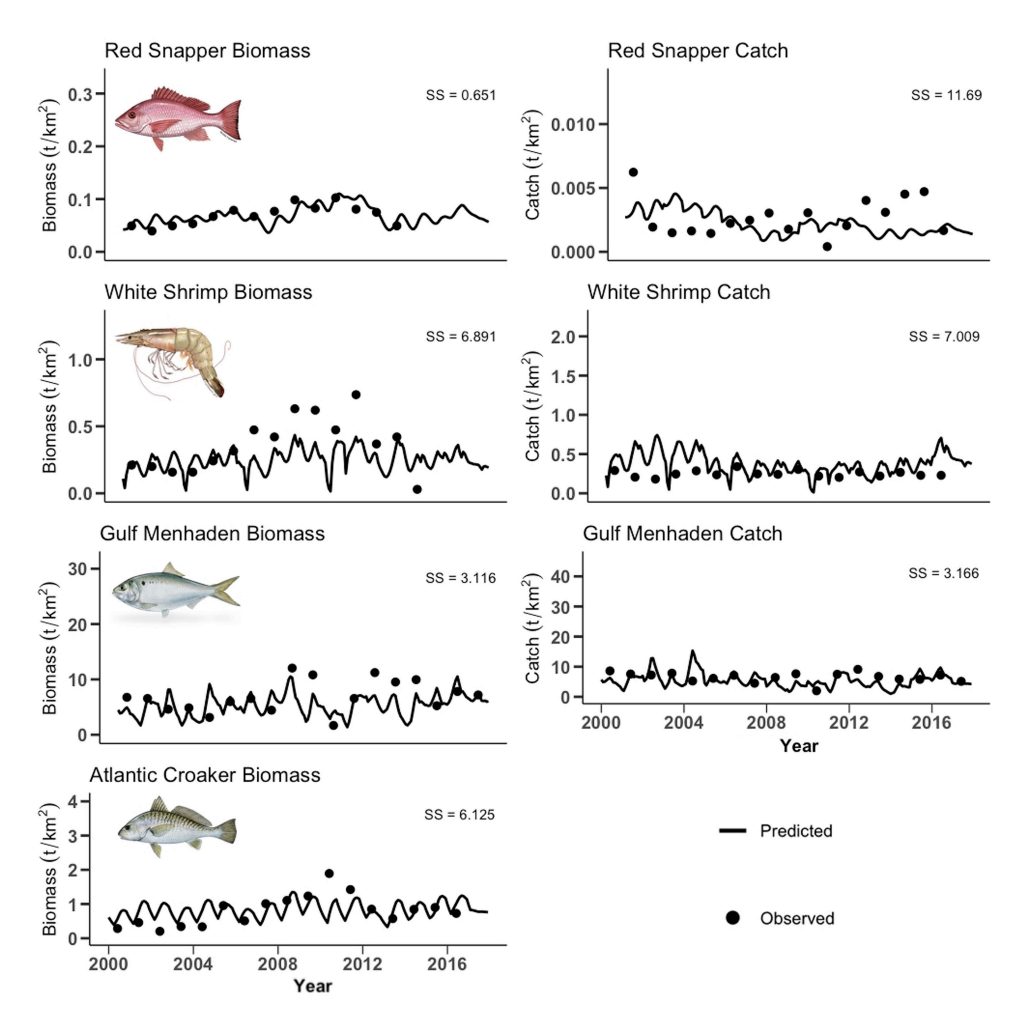


Figure 3. Calibration plots of the biomass and catch (metric tons [t]/km²) of the four focus species: Red Snapper, white shrimp, Gulf Menhaden, and Atlantic Croaker. There is no Atlantic Croaker fishery. The dots are the observed values, while the lines are predicted Ecosim output. The sum of squares (SS) value in each plot indicates the sum of squared differences between predicted and observed.

were calibrated for biomass, and 13 groups were calibrated for catch. The best-fit model was chosen as having the lowest value of Akaike's information criterion, and the model was adjusted until the lowest sum of squares between predicted and observed was reached (Figure 3).

The calibrated model was run in Ecospace, where all interactions occur in each model cell, and model cells are linked through the movement of organisms and fleets. The spatial feature of Ecospace allows for the evaluation of a spatial stressor, such as the hypoxic zone, and is especially suitable for spatial research questions like the ones posed here that relate to changes in the spatial extent of a stressor and where movement of organisms and fleets is a likely response to the stressor (De Mutsert et al., 2024). Simulations were run in individualbased model mode, which is an upgrade from De Mutsert et al. (2016). In individual-based model mode, spatial variations in consumption and mortality rates are predicted by dividing each multi-stanza population into a user-defined number of packets (also referred to as cohorts or superindividuals). Each packet represents a group of identical individuals of the same age and retains its own multi-stanza size-age structure. At the start of a simulation, all packets are initialized with identical monthly numbers-at-age and weight-at-age distributions, which are

then uniformly allocated across grid cells with habitat capacity exceeding 0.1. During each monthly time step, packets are tracked individually as they traverse grid cells. This approach allows for the calculation of the consumption and mortality rates of each packet based on the local environmental conditions in the cell occupied by the packet at the beginning of each time step. Consequently, packets can dynamically respond to spatial and temporal variations in ecological conditions (De Mutsert et al., 2024; Walters et al., 2010).

Linking the models

The models were linked offline by re-averaging the high-resolution NetCDF (Network Common Data Form) output of DO, phytoplankton, and temperature into ASCII files, providing one value per 5-km² Ecospace model grid cell per month, which is the time step in Ecospace model runs. For DO, the median value of the bottom layer with the lowest oxygen for each month was used per 5-km² grid cell; for phytoplankton, the median value of the top layer for each month was used per 5-km² grid cell. Temperature was used to include seasonality in the model, and the depth-integrated value of all vertical layers per 5-km² grid cell was used. The sets of ASCII files were stored on the local hard drive. At the start of each monthly time

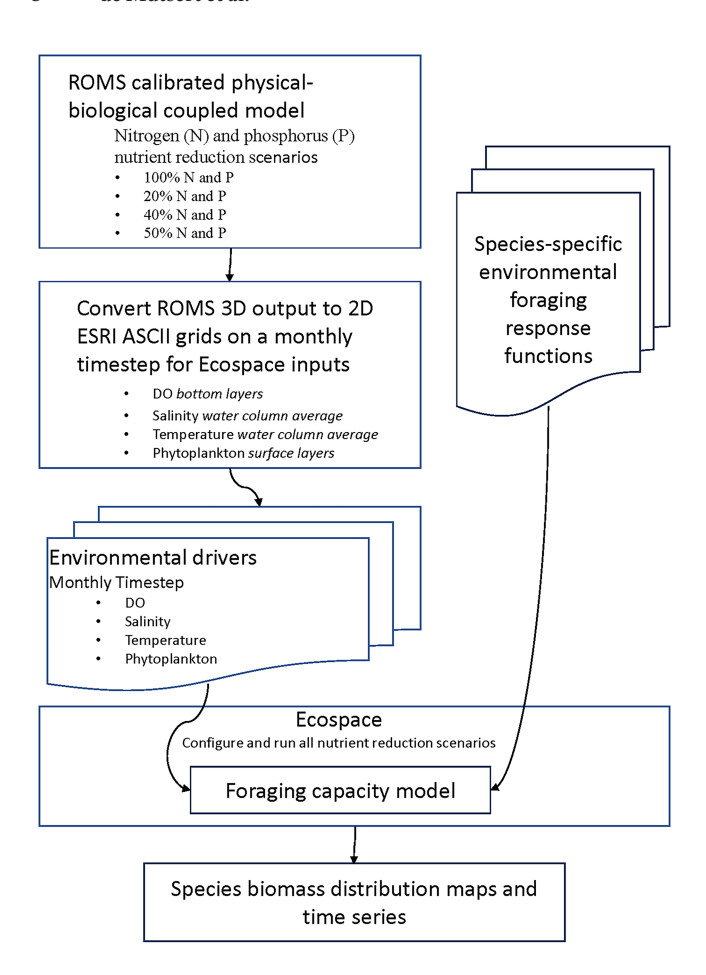


Figure 4. Model linking diagram. Abbreviations are as follows: ROMS = Regional Ocean Modeling System and DO = dissolved oxygen.

step of an Ecospace model run, the spatial—temporal model as described by Steenbeek et al. (2013) loaded the appropriate ASCII files for DO and temperature as environmental layer maps and the files for phytoplankton as primary production driver maps (Figure 4). An exclusion layer was applied over the Ecospace model area to exclude model cells that were not part of the physical—biological model; this was done to ensure that all Ecospace cells received environmental driver input from the physical—biological model (Figure 1).

Data from SEAMAP were used to determine the tolerance ranges of each species in the model to DO, temperature, and salinity. During SEAMAP surveys, these environmental variables are measured at the time of fish and shellfish collection. The catch rate plotted against each variable for each species or model group formed the basis for creating response curves in the model, as was first done in De Mutsert et al. (2012). The shape of the curve was predetermined for each variable: sigmoidal for DO and trapezoidal for temperature and salinity. These curves were fitted to the catch rate plots and were subsequently set to a y-axis of habitat capacity, as described by Christensen et al. (2014), to determine the suitability of the environmental conditions based on these three variables. The habitat capacity model described by Christensen et al. (2014) linked the environmental layers with species-specific response curves to determine the habitat capacity of each model cell for each time step for each species or model group. Habitat capacity affects feeding rate and movement (Christensen et al., 2014). The effect on movement allows for avoidance of unsuitable conditions by species in the model.

Scenarios simulated

After running the environmental conditions from the calibration run from 2000 to 2016 in Ecospace, we ran the following scenarios for another 17 years until 2035: no nutrient reductions, a 20% reduction in N&P load from the Mississippi River, a 40% reduction in N&P load, and a 50% reduction in N&P load. The environmental conditions from the physical-biological model for 2000-2016 represented the conditions of those actual years. The nutrient load reduction scenarios were created with the physical-biological model by running the years 2000–2016 again with all conditions the same except for the N&P loading into the system and the subsequent effects of the nutrient load reductions on phytoplankton and DO. In Ecospace, each scenario was run from 2000 to 2035. To create these 36-year scenarios in Ecospace, the DO, temperature, and phytoplankton output (without nutrient reduction) was first loaded from 2000 to 2016 and then the environmental parameter output from the 2000-2016 runs was either repeated for the baseline run or repeated under the selected nutrient load reductions. As such, all 36-year simulations received the same environmental conditions for the first 17 years (representing the calibrated years 2000–2016). This provides a spin-up period as well as a check that the model scenarios produce the same results if the same environmental conditions are received. Since the actual field conditions for the years 2017–2035 are not simulated but just the above-mentioned scenarios are run in those years, the results are presented as model years 0-35. To isolate the effects of hypoxia, all scenarios were run again but without the effect of the nutrient load reductions on primary production.

The spatial DO, phytoplankton, and temperature output was included in Ecospace by automatically loading a new ASCII grid file at the start of each monthly time step for the duration of the model run (see Figure 5 for examples). Each simulation was repeated using Monte Carlo simulations in which all Ecopath input parameters were varied with a CV of 0.1, and 100 successfully balanced models were run in Ecospace for each scenario to evaluate the uncertainty in each scenario. This is the first published extension of the Ecopath with Ecosim Monte Carlo routine into Ecospace, producing spatial Monte Carlo output (De Mutsert et al., 2024). Spatial probability density plots were created from the Monte Carlo output (Figure 6), and the SDs of the probability density plots of each model group from the no nutrient reduction simulations were included in the figures to visualize whether any of the nutrient reduction scenarios would result in biomass output falling 1 SD outside of the probable output from the baseline run (no nutrient reduction).

RESULTS

Hypoxia had a clear effect on the spatial distribution of nekton in the model. All focus species show reduced biomass in the hypoxic zone during the month of August, when hypoxia is present (Figures 5 and 7). This effect was diminished in nutrient

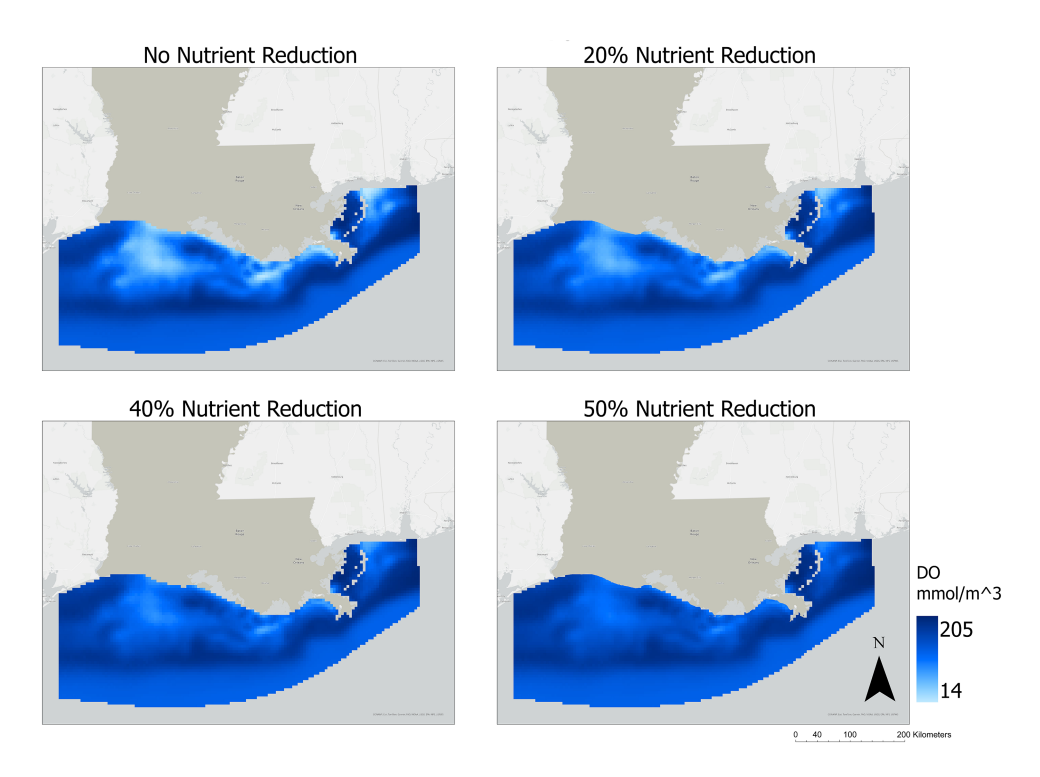


Figure 5. Dissolved oxygen (DO) output in August of the last simulation year of the physical-biological model under no nutrient reduction and 20, 40, and 50% nitrogen and phosphorus reductions.

reduction scenarios: The effect of the hypoxic zone decreased with each higher percentage nutrient reduction (20, 40, and 50% reductions in N&P). The effects of hypoxia on the spatial distribution of species were species-specific. Red Snapper showed a strong spatial displacement by hypoxia that diminished a bit more with each larger nutrient reduction. White shrimp were affected even a bit more spatially, with clear biomass hot spots in small areas near the coast where DO was not limiting. Those hot spots became larger under the nutrient reduction scenarios, while the general spatial displacement away from the coast was reduced. Small but clear hypoxia effects were still present at a 50% reduction in nutrients. Low DO affected Gulf Menhaden in a larger area, but the effect was less strong. The reduction of nutrients and hypoxia did alleviate the spatial displacement away from the coast, but even a 50% reduction in nutrients still showed an effect of hypoxia. The nutrient reductions also caused biomass hot spots of Gulf Menhaden near the coast in areas where DO increased enough to not be limiting. Hypoxia clearly affected the distribution of Atlantic Croaker but only when there was no nutrient reduction or a 20% nutrient reduction. The spatial displacement at those two scenarios also saw a concentration of biomass in spots right near the coast where the hypoxic zone was broken up. Compared to the scenario of no nutrient reduction, spatial displacement of Atlantic Croaker was reduced at the 20% nutrient reduction scenario and disappeared when the N&P load was reduced by 40% and 50% (Figure 7). Although the specific distribution patterns were different for all four species, the spatial displacement (avoidance) in response to hypoxia and the spatial distribution responses to nutrient reduction scenarios were clearly visible for all.

The effects on the average annual biomass (metric tons/km²) of all scenarios were small for all focus species (Figure 8). In

addition, the changes in fisheries species biomass in response to nutrient load reductions were species-specific and varied by year (Figure 8). Both reduced biomass and increased biomass were seen as a result of nutrient reduction scenarios. The largest nutrient reduction (50% N&P reduction) resulted in an annual average change (\pm SD) of $-3.9\pm4.45\%$ in Red Snapper biomass, $+3.5\pm4.96\%$ in white shrimp biomass, $+9.8\pm4.95\%$ in Gulf Menhaden biomass, and $-6.2\pm3.19\%$ in Atlantic Croaker biomass. The annual differences are most likely a result of the hypoxic zone size differences by year. The results of the uncertainty analysis of the base run showed that the increases and decreases in biomass as a result of the nutrient reduction scenarios often barely exceeded the uncertainty bounds (Figure 8).

Species-specific, year-specific, and small responses were observed for all groups in the model (Figures S1-S66 [see online Supplementary Material). Of the 66 model groups, the change in biomass did not exceed the uncertainty bounds in any year for 22 groups; the biomass dropped just below the uncertainty bounds in some years during a 50% nutrient reduction only for 20 groups; the biomass dropped below the uncertainty bounds in some years during both 50% and 40% nutrient reductions for 10 groups; the biomass dropped below the uncertainty bounds in some years during 50, 40, and 20% nutrient reductions for four groups; the biomass increased above the uncertainty bounds in some years during a 50% nutrient reduction only for two groups; the biomass increased above the uncertainty bounds in some years during both 50% and 40% nutrient reductions for six groups; and the biomass increased above the uncertainty bounds in some years during 50, 40, and 20% nutrient reductions for one group (Table 2; Figures S1–S66).

To determine whether the weak response to nutrient reduction scenarios was a result of the opposing effects of reduced

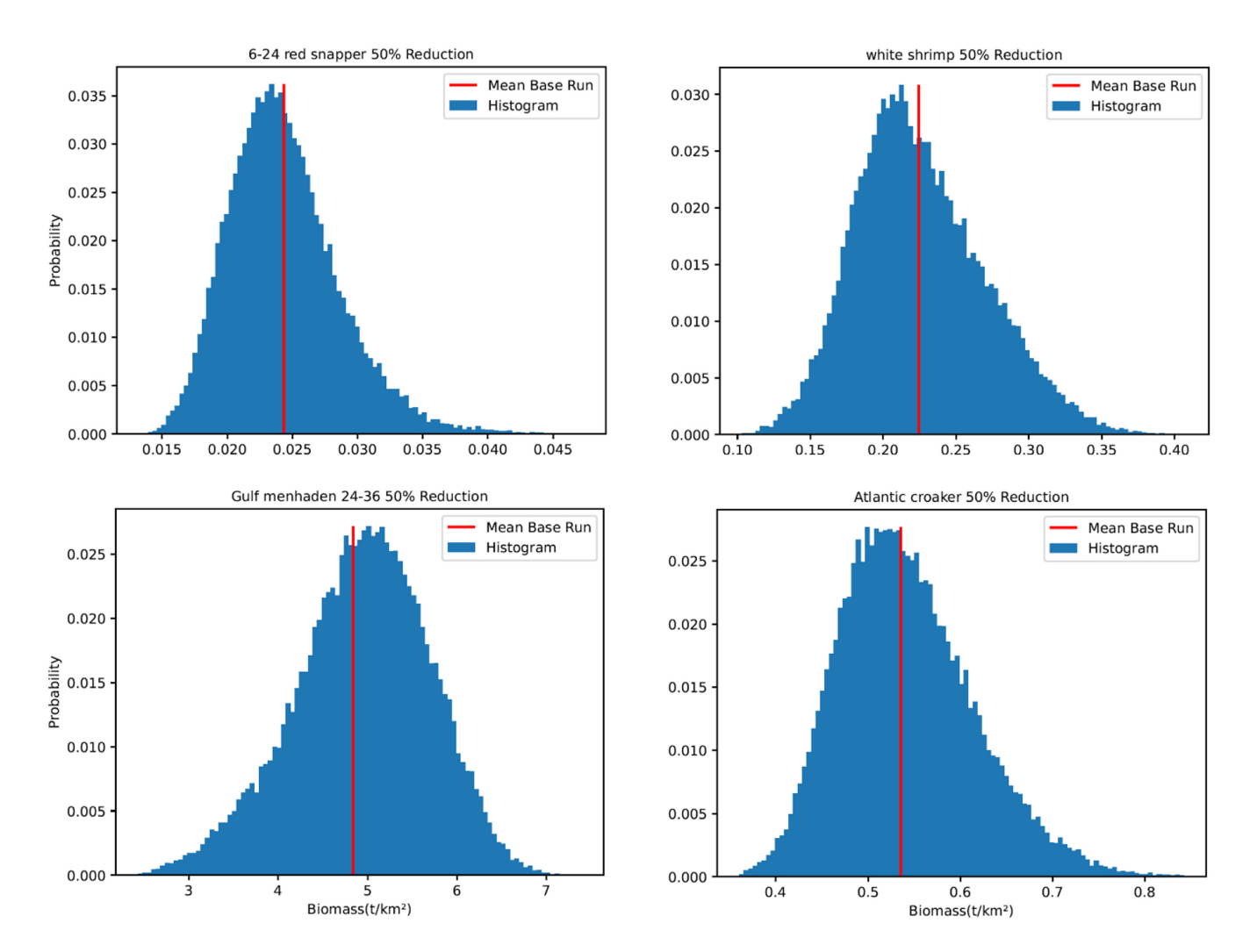


Figure 6. Probability density plots of spatial Monte Carlo run results. The plots of the 50% reduction in nitrogen and phosphorus are shown. Output biomass (metric tons $[t]/km^2$) is shown on the x-axis, and probability of occurrence is shown on the y-axis. The "Mean Base Run" line shows the base model run output. The numbers 6–24 (Red Snapper) and 24–36 (Gulf Menhaden) represent the age ranges of those groups in months.

hypoxia and reduced productivity on nekton biomass, the simulations were rerun, but the scenarios only reduced hypoxia, with no effects of nutrient reductions on phytoplankton. If only hypoxia is reduced under each of the N&P reduction scenarios, all biomass changes are positive, indicating that reduced productivity under reduced nutrient loading is responsible for the negative or small net effects of nutrient and hypoxia reductions on the biomass of living resources (Figure 9). Red Snapper switched from a decrease to an increase in biomass when only reduced hypoxia was considered, with both the 40% and 50% reduction scenarios showing biomass exceeding the uncertainty bounds in some years. White shrimp switched from alternating increases and decreases in biomass depending on the year (and all within the uncertainty bounds) to biomass increases in all years, with both the 40% and 50% nutrient reduction scenarios exceeding the uncertainty bounds. Gulf Menhaden switched from small increases in biomass in all scenarios, with only the 40% and 50% reduction scenarios barely exceeding the uncertainty bounds in some years, to clear biomass increases in all scenarios compared to the baseline, with the 40% and 50% reduction scenarios exceeding the

uncertainty bounds in all years. Atlantic Croaker switched from a decrease in biomass to an increase in biomass for all years, but all scenarios still fell within the uncertainty bounds.

DISCUSSION

Hypoxia had a clear effect on the spatial distribution of nekton in the model, and avoidance and biomass reduction in the hypoxic area were less when hypoxia was reduced. Avoidance is an important mechanism driving spatial distribution patterns; this is reflected in the model by reduced organism dispersal into areas from higher to lower habitat capacity and increased dispersal from lower to higher habitat capacity (Christensen et al., 2014). The spatial response of fisheries species to hypoxia in the northern Gulf of Mexico by leaving or avoiding the hypoxic zone has been shown by Craig (2012) and Purcell et al. (2017) through the distribution of fishing vessels along the edges of the hypoxic zone to target the high Gulf shrimp densities along these edges. Avoidance of stressors by motile marine organisms has been widely documented in the literature (Chapman & Mckenzie, 2009; Vilas et al., 2023; Yu et al., 2023). That the

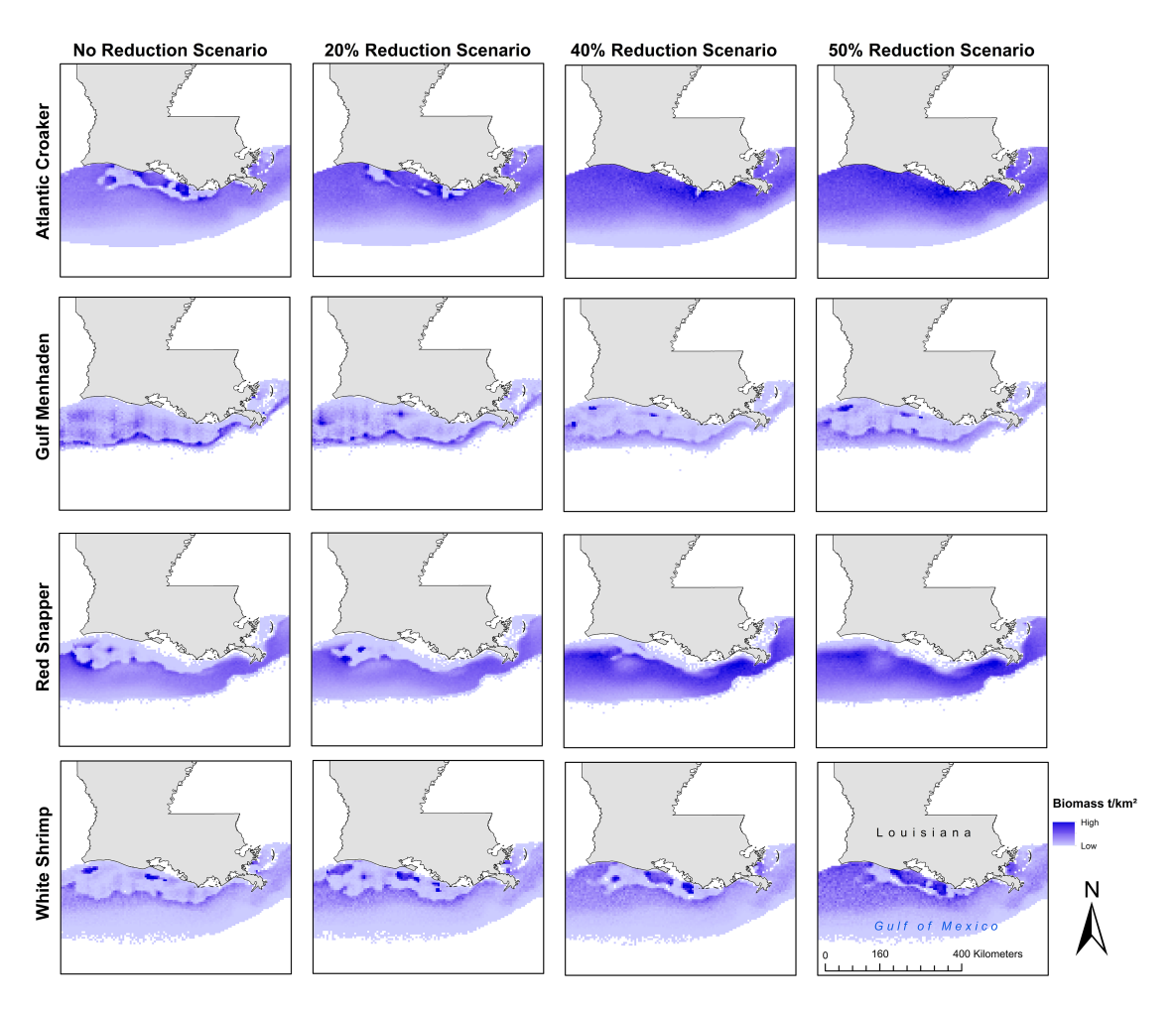


Figure 7. Spatial biomass (metric tons $[t]/km^2$) distribution output at the end of the simulation scenarios in a month when the hypoxic zone is present (August of model year 2035) for Red Snapper, white shrimp, Gulf Menhaden, and Atlantic Croaker under no nutrient reduction and 20, 40, and 50% reductions in nitrogen and phosphorus load. Darker colors indicate more biomass.

biomass reduction in the hypoxic areas is the combined result of reduced biomass production and avoidance is one of the reasons why the spatial displacement of biomass can be significant, while the changes in total biomass are not. In addition to that, the aggregation at the edges of hypoxic areas can create biomass hot spots (Craig, 2012; Craig & Crowder, 2005), and the physical–biological model simulations and the nekton response show that the hypoxic zone is not a uniform area but is shaped irregularly, exhibiting spots with high DO.

Because the reduction in hypoxia is achieved by a reduction in nutrient loading, there are also less nutrients to fuel primary production and subsequently secondary production. In addition to spatial displacement and avoidance as discussed above, the opposing effects of hypoxia and nutrient reductions are an important reason for the small positive or even small negative effects of nutrient load reductions on fisheries species biomass. Annual average biomass output shows that changes in fish and shellfish biomass in response to nutrient load reductions are small and species-specific and that they vary by year. Previous studies have shown that nutrient enrichments accompanied by increased hypoxia do not reduce fisheries landings for the same reason (Breitburg et al., 2009); therefore, it may be expected that nutrient reductions do not increase biomass or landings.

A similar study in Europe that evaluated effects of management measures to reduce N loading to marine environments showed that the proposed nutrient reduction measures had no impact on most assessed criteria in marine environments and had small negative effects on commercial fish stocks and small forage fish biomass (Piroddi et al., 2021). When we isolated the effects of hypoxia in our simulations, all biomass changes were positive, indicating that reduced productivity under reduced nutrient loading is responsible for the negative or small net effects of nutrient and hypoxia reductions on the biomass of living resources. While it is insightful to isolate the effect of hypoxia reductions on biomass, including the effects of the nutrient reductions on primary productivity and subsequently secondary productivity creates output that is a more realistic expectation of the effects. We used novel spatial Monte Carlo simulations in Ecospace to create the uncertainty bounds. This method tests how the biomass output of each model group might change when all Ecopath input parameters are varied within a CV of 0.1. This process affected the biomass of each model group during each time step in each model cell, the last of which is new since Monte Carlo simulations have so far only been run in Ecosim, the time-dynamic module of Ecopath with Ecosim. This approach served more than one purpose.

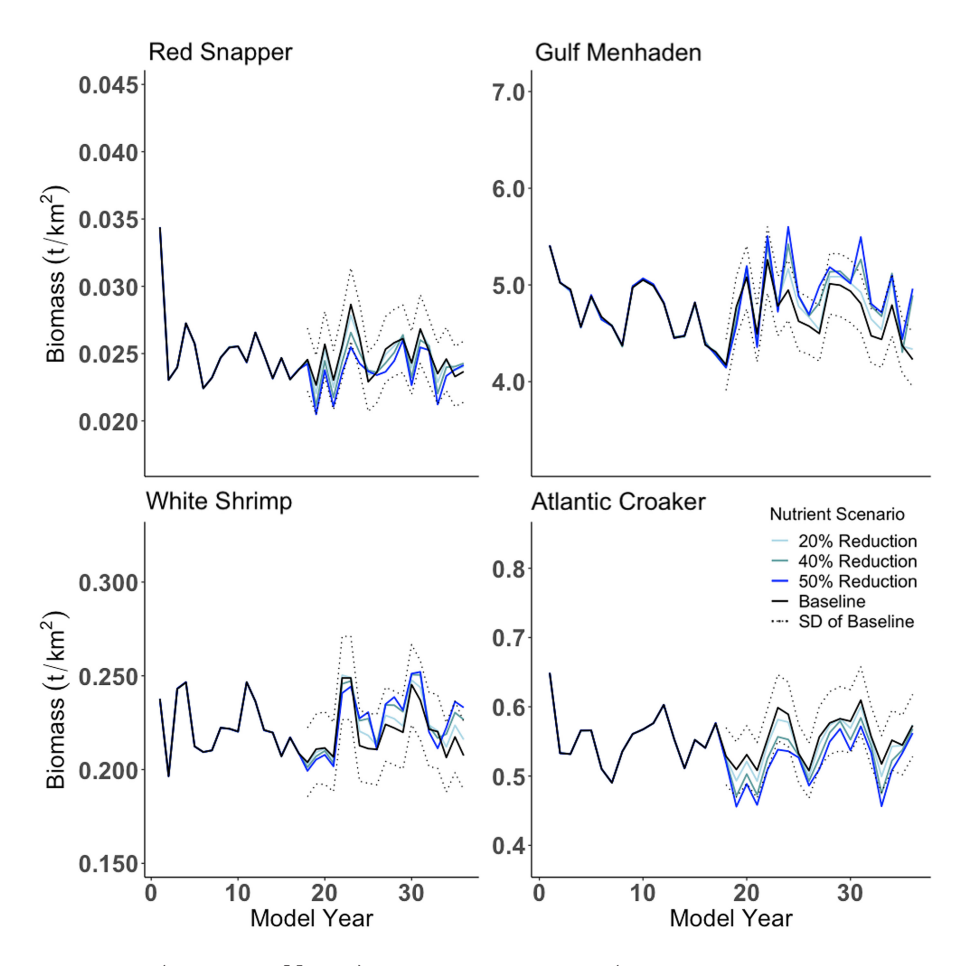


Figure 8. Average annual biomass (metric tons $[t]/km^2$) of the four focus species (Red Snapper, white shrimp, Gulf Menhaden, and Atlantic Croaker) in all scenarios for the duration of the model runs. The SDs of the probability density plots of the baseline run are indicated with the dotted lines.

We were able to show with probability density plots that the provided output falls within the most likely output when small variations in input values are applied and that the probability is distributed normally. This shows that the model is robust to small input change in start biomass and turnover rates (the parameters of which we are unable to know the exact value) even when the scenario most different from the baseline was run (50% nutrient load reduction). For the uncertainty bounds, we used the SD of probability density plots of the baseline run for each model group to determine the range within which the baseline output probably occurs with small changes in input parameters. We determined that if the scenario output falls within this range, the difference from the baseline run is small. Since we cannot truly test whether the differences are significant or not, we provide all output and uncertainty bounds in plots, thus allowing users to make their own evaluation.

The nutrient reduction scenarios tested are relevant management scenarios since they are the nutrient reduction goals of the HTF (U.S. Environmental Protection Agency, 2025). To promote relevance and uptake of our result, the model was co-produced, and selected scenarios and output metrics were discussed with an advisory panel that included members of the HTF; this process was described by Shaffer et al. (2023). The uncertainty analysis revealed that none of the nutrient reduction scenarios affected the biomass of fisheries species to

such an extent that it transcended the uncertainty bounds of the base run of no nutrient reductions. The proposed nutrient reductions are thereby not expected to significantly affect the total annual biomass of fisheries species in the northern Gulf of Mexico ecosystem, but they will affect the distribution by increasing fisheries species biomass closer to the coast.

There could be ecological and socioeconomic consequences of distribution shifts closer to the coast of fish and shellfish species targeted by the fishing industry (Smith et al., 2014). Such shifts may increase interactions with estuarine habitats, where increased fishing pressure could disrupt nursery functions, alter food web dynamics, and elevate bycatch of juvenile and nontarget species (Craig & Bosman, 2013; Minello et al., 2003). Economically, inshore shifts could benefit some fisheries through reduced fuel costs and increased access but may also reduce the overall resilience of stocks by concentrating effort in more vulnerable habitats (Langseth et al., 2014). Therefore, spatial distribution shifts potentially require new management strategies, spatial protections, and monitoring systems to mitigate localized depletion and preserve ecosystem services.

It is important to note that the modeling approach is able to simulate the effects of hypoxia and nutrient loading (and changes therein) on the spatial distribution through movement and the total biomass and spatial distribution of biomass of model groups through changes in feeding rate, while other

Table 2. Model groups listed based on the effect that the 50, 40, and 20% nutrient reduction scenarios had on the biomass of the group. Columns indicate whether the change in biomass remained within the uncertainty bounds, which refers to the SD of the probability density plots of the baseline output obtained using Monte Carlo simulations, or moved above or below the uncertainty bounds for one (50%) nutrient reduction scenario, some (50% and 40%) scenarios, or all (50, 40, and 20%) scenarios. The numbers associated with some of the model group names refer to age-classes in months for multi-stanza groups. These results are visualized in Figures S1–S66.

Within uncertainty boundsBelow uncertainty bound in 50% reductionuncertainty bound in 50% and 40% reductionsuncertainty 40, and 20% reductionsAbove uncertainty bound in 50% and 40% reductionuncertainty and 40% 40, and 20% reductionsbound in 50% and 40% reductionuncertainty uncertainty bound in 50% and 40% do, and 20% reductionsMarine mammalsCarangidae0-3 Red Drum Juvenile Atlantic Cutlassfish Cutlassfish and skatesAtlantic Bumper Small forage fish and skates36+ Gulf MenhadenJuvenile King MackerelJuvenile King MackerelAtlantic CutlassfishAtlantic CutlassfishLizardfish0-3 seatrout CutlassfishScadDetritus9-12 Gulf MenhadenJuvenile sharks6-24 Red SnapperJuvenile ButterfishDetritus9-12 Gulf MenhadenJuvenile Spanish Mackerel3-8 Red Drum 18+ seatroutSquid24+ Red Snapper 0-12 Serranidae 12-36 Serranidae Rays and skates Catfish Duvenile brown shrimp Juvenile brown shrimp Juvenile brown shrimp Juvenile brown shrimp Hownile white shrimp White shrimpAtlantic Croaker Sea turtles Blue crab Other shrimp PhytoplanktonBerthic algae	- 3 1			0 1			
Tunas Juvenile Atlantic Cutlassfish and skates arrout Flounders Soughly Flounders Flounders Soughly Flounders Flounder	,	uncertainty bound in 50%	uncertainty bound in 50% and 40%	uncertainty bound in 50, 40, and 20%	uncertainty bound in 50%	uncertainty bound in 50% and 40%	Above uncertainty bound in 50, 40, and 20% reductions
TunasJuvenile Atlantic CutlassfishJuvenile rays and skatesSmall forage fish and skatesPink shrimp CutlassfishAtlantic CutlassfishBirds0-3 seatroutFloundersZooplanktonSpanish MackerelLizardfish0-6 Red SnapperDetritus0-12 Gulf MenhadenJuvenile sharks6-24 Red SnapperJuvenile Butterfish12-24 Gulf MenhadenSharksOther snappersButterfish24-36 Gulf MenhadenJuvenile Spanish Mackerel3-8 Red DrumSquid3-18 seatrout8-18 Red DrumPorgies24+ Red Snapper36+ Red DrumPorgies24+ Red SnapperJuvenile Atlantic CroakerBenthic algae0-12 SerranidaeJuvenile Atlantic Croaker12-36 SerranidaeAtlantic Croaker36+ SerranidaeAnchovyCatfishClupeidsJuvenile brown shrimpMulletBrown shrimpSea turtlesJuvenile white shrimpOther shrimpWhite shrimpOther shrimpJuvenile pink shrimpPhytoplankton	Marine mammals	Carangidae	0–3 Red Drum	Atlantic Bumper			King Mackere
Lizardfish O-6 Red Snapper Scad Detritus O-12 Gulf Menhaden Juvenile sharks 6-24 Red Snapper Butterfish Menhaden Snapper Butterfish Menhaden Snapper Butterfish Menhaden Sharks Other snappers Butterfish Menhaden Juvenile Spanish 3-8 Red Drum Squid Mackerel 3-18 seatrout 18-36 Red Drum Pinfish 18+ seatrout 18-36 Red Drum Porgies 24+ Red Snapper 36+ Red Drum Jellyfish O-12 Serranidae Juvenile Atlantic Croaker 12-36 Serranidae Spot Spot Rays and skates Anchovy Catfish Clupeids Juvenile brown shrimp Mullet Brown shrimp Sea turtles Juvenile white shrimp Other shrimp Other shrimp Juvenile pink shrimp Phytoplankton Detritus O-12 Gulf Menhaden 12-24 Gulf Menhaden 12-25 Gulf Menhaden 12-26 Gu	Tunas	2	,	Small forage fish		Atlantic	
Juvenile sharks 6-24 Red Snapper Butterfish Menhaden 12-24 Gulf Menhaden 12-36 Gulf Menhaden Juvenile Spanish Menhaden Juvenile Spanish Menhaden Juvenile Spanish Menhaden Juvenile Spanish Menhaden Squid Juvenile Spanish Menhaden Squid Juvenile Spanish Menhaden Squid Juvenile Spanish Menhaden Squid Squ	Birds	0-3 seatrout	Flounders	Zooplankton		Spanish Mackerel	
Juvenile sharks6-24 Red SnapperJuvenile Butterfish12-24 Gulf MenhadenSharksOther snappersButterfishMenhadenJuvenile Spanish Mackerel3-8 Red Drum MackerelSquid3-18 seatrout8-18 Red Drum PinfishPinfish18+ seatrout18-36 Red Drum PorgiesPorgies24+ Red Snapper36+ Red Drum JellyfishBenthic algae0-12 SerranidaeJuvenile Atlantic CroakerBenthic algae36+ SerranidaeSpotSenthic algaeRays and skatesAnchovyAnchovyCatfishClupeidsJuvenile brown shrimpMulletBrown shrimpSea turtlesJuvenile white shrimpBlue crabWhite shrimpOther shrimpPhytoplankton	Lizardfish	0-6 Red Snapper	Scad	Detritus		0–12 Gulf	
Snapper Butterfish Menhaden Sharks Other snappers Butterfish 24–36 Gulf Menhaden Juvenile Spanish 3–8 Red Drum Squid Mackerel 3–18 seatrout 8–18 Red Drum Pinfish 18+ seatrout 18–36 Red Drum Porgies 24+ Red Snapper 36+ Red Drum Jellyfish 0–12 Serranidae Juvenile Atlantic Croaker 12–36 Serranidae Atlantic Croaker 36+ Serranidae Spot Rays and skates Anchovy Catfish Clupeids Juvenile brown shrimp Mullet Brown shrimp Sea turtles Juvenile white shrimp Blue crab White shrimp Other shrimp White shrimp Phytoplankton						Menhaden	
Sharks Other snappers Butterfish 24–36 Gulf Menhaden Juvenile Spanish Mackerel 3–18 seatrout 8–18 Red Drum Pinfish 18+ seatrout 18–36 Red Drum Porgies 24+ Red Snapper 36+ Red Drum Jellyfish 0–12 Serranidae Juvenile Atlantic Croaker 12–36 Serranidae Atlantic Croaker 36+ Serranidae Spot Rays and skates Anchovy Catfish Clupeids Juvenile brown shrimp Mullet Brown shrimp Sea turtles Juvenile white shrimp Blue crab White shrimp Other shrimp Juvenile pink shrimp Phytoplankton	Juvenile sharks	6-24 Red	Juvenile			12-24 Gulf	
Juvenile Spanish Mackerel 3–18 seatrout 18–36 Red Drum Pinfish 18+ seatrout 18–36 Red Drum Porgies 24+ Red Snapper 36+ Red Drum Jellyfish 0–12 Serranidae Uvenile Atlantic Croaker 12–36 Serranidae 35+ Serranidae 36+ S		Snapper	Butterfish			Menhaden	
Juvenile Spanish Mackerel3–8 Red Drum MackerelSquid3–18 seatrout8–18 Red Drum Pinfish18+ seatrout18–36 Red Drum Porgies24+ Red Snapper36+ Red Drum Jellyfish0–12 SerranidaeJuvenile Atlantic Croaker12–36 SerranidaeAtlantic Croaker36+ SerranidaeSpotRays and skatesAnchovyCatfishClupeidsJuvenile brown shrimpMulletBrown shrimpSea turtlesJuvenile white shrimpBlue crabWhite shrimpOther shrimpJuvenile pink shrimpPhytoplankton	Sharks	Other snappers	Butterfish				
18+ seatrout 24+ Red Snapper 36+ Red Drum O-12 Serranidae Juvenile Atlantic Croaker 12-36 Serranidae Atlantic Croaker 36+ Serranidae Spot Rays and skates Anchovy Catfish Clupeids Juvenile brown shrimp Brown shrimp Brown shrimp Brown shrimp Sea turtles Juvenile white shrimp White shrimp Juvenile pink shrimp Other shrimp Phytoplankton Porgies Jellyfish Benthic algae Enthic algae Croaker Senthic algae Croaker Other shrimp Senthic algae		3–8 Red Drum	Squid			Weimaden	
24+ Red Snapper 0-12 Serranidae	3-18 seatrout	8-18 Red Drum	Pinfish				
24+ Red Snapper 0-12 Serranidae Uvenile Atlantic Croaker 12-36 Serranidae 36+ Serranidae 36+ Serranidae 36+ Serranidae Atlantic Croaker Spot Rays and skates Catfish Clupeids Juvenile brown shrimp Brown shrimp Brown shrimp Sea turtles Juvenile white shrimp White shrimp Juvenile pink shrimp Phytoplankton Jellyfish Benthic algae Benthic algae Senthic algae Benthic algae Benthic algae Senthic algae Benthic algae Benth	18+ seatrout	18-36 Red Drum	Porgies				
0–12 Serranidae	24+ Red Snapper	36+ Red Drum					
36+ SerranidaeSpotRays and skatesAnchovyCatfishClupeidsJuvenile brown shrimpMulletBrown shrimpSea turtlesJuvenile white shrimpBlue crabWhite shrimpOther shrimpJuvenile pink shrimpPhytoplankton		2	- ,				
Rays and skates Anchovy Catfish Clupeids Juvenile brown shrimp Mullet Brown shrimp Sea turtles Juvenile white shrimp Blue crab White shrimp Other shrimp Juvenile pink shrimp Phytoplankton	12-36 Serranidae	Atlantic Croaker					
Rays and skatesAnchovyCatfishClupeidsJuvenile brown shrimpMulletBrown shrimpSea turtlesJuvenile white shrimpBlue crabWhite shrimpOther shrimpJuvenile pink shrimpPhytoplankton	36+ Serranidae	Spot					
Juvenile brown shrimp Brown shrimp Sea turtles Juvenile white shrimp White shrimp Other shrimp Juvenile pink shrimp Phytoplankton	Rays and skates						
Juvenile brown shrimpMulletBrown shrimpSea turtlesJuvenile white shrimpBlue crabWhite shrimpOther shrimpJuvenile pink shrimpPhytoplankton	,	,					
Brown shrimp Sea turtles Juvenile white shrimp Blue crab White shrimp Other shrimp Juvenile pink shrimp Phytoplankton	Juvenile brown shrimp	1					
Juvenile white shrimpBlue crabWhite shrimpOther shrimpJuvenile pink shrimpPhytoplankton	-	Sea turtles					
White shrimp Other shrimp Juvenile pink shrimp Phytoplankton	1	Blue crab					
Juvenile pink shrimp Phytoplankton	-	Other shrimp					
	Juvenile pink shrimp	•					
Benthic crabs	Benthic crabs	, ,					
Benthic invertebrates	Benthic invertebrates						

effects, such as changes in individual growth rates, individual reproductive potential, and community composition, are not simulated. Although no model simulates all potential effects, an ensemble modeling approach whereby different types of models simulate effects of the same scenarios on higher trophic levels, while mechanistically different and generating different types of output, would provide a more wholistic picture of the effects of the HTF's nutrient reduction goals. Since other modeling efforts have been underway during the same time frame as this work (S. Brandt, Oregon State University, and K. Rose, University of Maryland Center for Environmental Science, personal communication), a synthesis paper of these three efforts would be able to provide some resolution to these limitations.

To facilitate the use of the results of this simulation study, a decision support tool has been developed to visualize the model output for members of the HTF, fisheries managers, and other stakeholders (Shaffer et al., 2023). Users can select the nutrient reduction scenario (50, 40, or 20% reduction or no reduction) and can select the years, months, and fisheries species (Atlantic Croaker, brown shrimp Farfantepenaeus aztecus, Gulf Menhaden, Red Snapper, and white shrimp) for which to see biomass distribution maps and average biomass per year

throughout the simulations. The phytoplankton and DO concentration and distribution representing the environmental conditions of the selected scenario are shown as well.

In conclusion, hypoxia affects species distribution, which leads to additional indirect effects of hypoxia. For most of the fisheries species that we simulated, distribution is more strongly affected than total biomass. Nutrient load reductions reduce bottom-up energy flow into the food web, thus reducing secondary production. Associated hypoxia reductions have positive effects on fisheries species and most other groups in the food web. The net effect on living marine resource biomass is small and species-specific, and it varies by year. While total biomass might not be strongly affected by nutrient and hypoxia reductions, our simulations show expected effects on fisheries species distribution, placing fisheries species closer to shore in higher densities, which would have effects on important fisheries, such as the shrimp and Gulf Menhaden fishing industry.

SUPPLEMENTARY MATERIAL

Supplementary material is available at Marine and Coastal Fisheries online.

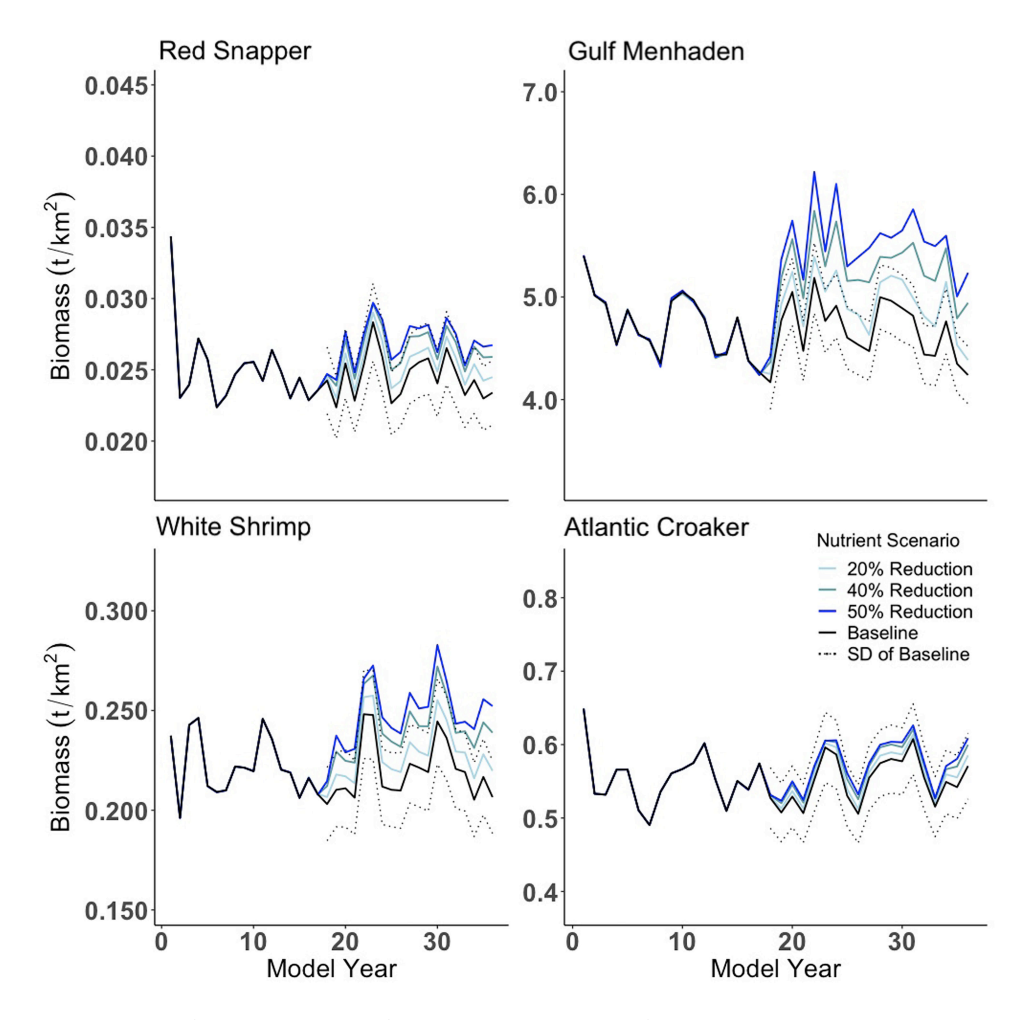


Figure 9. Average annual biomass (metric tons $[t]/km^2$) of the four focus species (Red Snapper, white shrimp, Gulf Menhaden, and Atlantic Croaker) in all scenarios for the duration of the model runs. In these scenarios, only hypoxia is reduced, while the nutrient loading is kept the same. The SDs of the probability density plots of the baseline run are indicated with the dotted lines.

DATA AVAILABILITY

No new data were collected for this study. Databases with available data used to develop the ecosystem model included SEAMAP (https://www.fisheries.noaa.gov/southeast/funding-and-financial-services/southeast-area-monitoring-and-assessment-program-seamap), FishBase (https://www.fishbase.se/home.htm), and SeaLifeBase (https://www.seal-ifebase.ca/Search.php). Stock assessment data used for Gulf Menhaden are not publicly available and cannot be legally shared by the authors. The ecosystem model will be uploaded to an open model repository upon publication (https://ecobase.ecopath.org/index.php?action=base).

ETHICS STATEMENT

This research meets the ethical guidelines and legal requirements of the countries (United States and Canada) in which it was performed.

FUNDING

This research was funded by the NOAA National Ocean Service under grant number NA16NOS4780202.

CONFLICTS OF INTEREST

None declared.

ACKNOWLEDGMENTS

We acknowledge SEAMAP for the use of survey data and FishBase and SeaLifeBase for the use of published parameters in our ecosystem model. We thank project collaborators Stephen Brandt, David Chagaris, Kris Lewis, Alex Van Plantinga, Cassie Glaspie, and Skyler Sagarese for their participation in and improvement of this work. We are grateful to all members of the advisory panel for their input and feedback. We appreciate the two anonymous reviewers who improved the manuscript with constructive criticism.

REFERENCES

Aulenbach, B. T., Buxton, H. T., Battaglin, W. A., & Coupe, R. H. (2007). Streamflow and nutrient fluxes of the Mississippi-Atchafalaya River basin and subbasins for the period of record through 2005 (Open-File Report 2007-1080). U.S. Geological Survey.

Bentley, J. W., Chagaris, D., Coll, M., Heymans, J. J., Serpetti, N., Walters, C. J., & Christensen, V. (2024). Calibrating ecosystem models to support ecosystem-based management of marine

- systems. ICES Journal of Marine Science, 81, 260–275. https://doi.org/10.1093/icesjms/fsad213
- Bentley, J. W., Lundy, M. G., Howell, D., Beggs, S. E., Bundy, A., de Castro, F., Fox, C. J., Heymans, J. J., Lynam, C. P., Pedreschi, D., Schuchert, P., Serpetti, N., Woodlock, J., & Reid, D. G. (2021). Refining fisheries advice with stock-specific ecosystem information. *Frontiers in Marine Science*, 8, Article 602072. https://doi.org/10.3389/fmars.2021.602072
- Breitburg, D. (2002). Effects of hypoxia, and the balance between hypoxia and enrichment, on coastal fishes and fisheries. *Estuaries*, 25, 767–781. https://doi.org/10.1007/BF02804904
- Breitburg, D. L., Craig, J. K., Fulford, R. S., Rose, K. A., Boynton, W. R., Brady, D. C., Ciotti, B. J., Diaz, R. J., Friedland, K. D., Hagy, J. D., Hart, D. R., Hines, A. H., Houde, E. D., Kolesar, S. E., Nixon, S. W., Rice, J. A., Secor, D. H., & Targett, T. E. (2009). Nutrient enrichment and fisheries exploitation: Interactive effects on estuarine living resources and their management. *Hydrobiologia*, 629, 31–47. https://doi.org/10.1007/s10750-009-9762-4
- Chagaris, D., Drew, K., Schueller, A., Cieri, M., Brito, J., & Buchheister, A. (2020). Ecological reference points for Atlantic Menhaden established using an ecosystem model of intermediate complexity. Frontiers in Marine Science, 7, Article 606417. https://doi.org/10. 3389/fmars.2020.606417
- Chapman, L. J., & Mckenzie, D. J. (2009). Behavioral responses and ecological consequences. In J. G. Richards, A. P. Farrell, & C. J. Brauner (Eds.), *Hypoxia* (Fish Physiology 27, pp. 25–77). Academic Press.
- Christensen, V., Coll, M., Steenbeek, J., Buszowski, J., Chagaris, D., & Walters, C. J. (2014). Representing variable habitat quality in a spatial food web model. *Ecosystems*, 17, 1397–1412. https://doi.org/10.1007/s10021-014-9803-3
- Christensen, V., & Walters, C. J. (2004). Ecopath with Ecosim: Methods, capabilities and limitations. *Ecological Modelling*, 172, 109–139. https://doi.org/10.1016/j.ecolmodel.2003.09.003
- Christensen, V., & Walters, C. J. (2024). Ecosystem modelling with EwE. University of British Columbia.
- Craig, J. K. (2012). Aggregation on the edge: Effects of hypoxia avoidance on the spatial distribution of brown shrimp and demersal fishes in the northern Gulf of Mexico. *Marine Ecology Progress Series*, 445, 75–95. https://doi.org/10.3354/meps09437
- Craig, J. K., & Bosman, S. H. (2013). Small spatial scale variation in fish assemblage structure in the vicinity of the northwestern Gulf of Mexico hypoxic zone. *Estuaries and Coasts*, 36, 268–285. https://doi.org/10.1007/s12237-012-9577-9
- Craig, J. K., & Crowder, L. B. (2005). Hypoxia-induced habitat shifts and energetic consequences in Atlantic Croaker and brown shrimp on the Gulf of Mexico shelf. *Marine Ecology Progress Series*, 294, 79–94. https://doi.org/10.3354/meps294079
- da Silva, A. P., Kay, B. D., & Perfect, E. (1994). Characterization of the least limiting water range of soils. Soil Science Society of America Journal, 58, 1775–1781. https://doi.org/10.2136/sssaj1994. 03615995005800060028x
- De Mutsert, K., Coll, M., Steenbeek, J., Ainsworth, C., Buszowski, J., Chagaris, D., Christensen, V., Heymans, S. J. J., Lewis, K. A., Libralato, S., Oldford, G., Piroddi, C., Romagnoni, G., Serpetti, N., Spence, M. A., & Walters, C. (2024). Advances in spatial-temporal coastal and marine ecosystem modeling using Ecospace. In D. Baird & M. Elliot (Eds.), Treatise on estuarine and coastal science (Vol. 5, 2nd ed., pp. 122–169). Elsevier.
- De Mutsert, K., Cowan, J. H., & Walters, C. J. (2012). Using Ecopath with Ecosim to explore nekton community response to freshwater diversion into a Louisiana estuary. Marine and Coastal Fisheries: Dynamics, Management, and Ecosystem Science, 4, 104–116. https://doi.org/10.1080/19425120.2012.672366
- De Mutsert, K., Steenbeek, J., Lewis, K., Buszowski, J., Cowan, J. H., & Christensen, V. (2016). Exploring effects of hypoxia on fish and fisheries in the northern Gulf of Mexico using a dynamic spatially explicit ecosystem model. *Ecological Modelling*, 331, 142–150. https://doi.org/10.1016/j.ecolmodel.2015.10.013

- Fennel, K., Hetland, R., Feng, Y., & DiMarco, S. (2011). A coupled physical-biological model of the northern Gulf of Mexico shelf: Model description, validation and analysis of phytoplankton variability. *Biogeosciences*, 8, 1881–1899. https://doi.org/10.5194/bg-8-1881-2011
- Fennel, K., Hu, J., Laurent, A., Marta-Almeida, M., & Hetland, R. (2013). Sensitivity of hypoxia predictions for the northern Gulf of Mexico to sediment oxygen consumption and model nesting. Journal of Geophysical Research: Oceans, 118, 990–1002. https://doi.org/10.1002/jgrc.20077
- Fennel, K., & Laurent, A. (2018). N and P as ultimate and proximate limiting nutrients in the northern Gulf of Mexico: Implications for hypoxia reduction strategies. *Biogeosciences*, *15*, 3121–3131. https://doi.org/10.5194/bg-15-3121-2018
- Fennel, K., Wilkin, J., Levin, J., Moisan, J., O'Reilly, J., & Haidvogel, D. (2006). Nitrogen cycling in the Middle Atlantic Bight: Results from a three-dimensional model and implications for the North Atlantic nitrogen budget. *Global Biogeochemical Cycles*, 20, Article GB3007. https://doi.org/10.1029/2005GB002456
- Fennel, K., Wilkin, J., Previdi, M., & Najjar, R. (2008). Denitrification effects on air–sea CO₂ flux in the coastal ocean: Simulations for the northwest North Atlantic. *Geophysical Research Letters*, 35, Article L24608. https://doi.org/10.1029/2008GL036147
- Geers, T. M., Pikitch, E. K., & Frisk, M. G. (2016). An original model of the northern Gulf of Mexico using Ecopath with Ecosim and its implications for the effects of fishing on ecosystem structure and maturity. *Deep-Sea Research Part II: Topical Studies in Oceanography*, 129, 319–331. https://doi.org/10.1016/j.dsr2.2014.01.009
- Glaspie, C. N., Clouse, M., Huebert, K., Ludsin, S. A., Mason, D. M., Pierson, J. J., Roman, M. R., & Brandt, S. B. (2019). Fish diet shifts associated with the northern Gulf of Mexico hypoxic zone. Estuaries and Coasts, 42, 2170–2183. https://doi.org/10.1007/s12237-019-00626-x
- Gulf Data, Assessment, and Review. (2013). GDAR 01—Stock assessment report Gulf of Mexico Blue Crab. Gulf States Marine Fisheries Commission.
- Haidvogel, D. B., Arango, H., Budgell, W. P., Cornuelle, B. D., Curchitser, E., Di Lorenzo, E., Fennel, K., Geyer, W. R., Hermann, A. J., Lanerolle, L., Levin, J., McWilliams, J. C., Miller, A. J., Moore, A. M., Powell, T. M., Shchepetkin, A. F., Sherwood, C. R., Signell, R. P., Warner, J. C., & Wilkin, J. (2008). Ocean forecasting in terrain-following coordinates: Formulation and skill assessment of the Regional Ocean Modeling System. *Journal of Computational Physics*, 227, 3595–3624. https://doi.org/10.1016/j.jcp.2007.06.016
- Hart, R. A. (2015a). Stock assessment update for brown shrimp (Farfantepenaeus aztecus) in the U.S. Gulf of Mexico for 2014. National Oceanic and Atmospheric Administration.
- Hart, R. A. (2015b). Stock assessment update for white shrimp (Litopenaeus setiferus) in the U.S. Gulf of Mexico for 2014. National Oceanic and Atmospheric Administration.
- Hart, R. A. (2015c). Stock assessment update for pink shrimp (Farfantepenaeus duorarum) in the U.S. Gulf of Mexico for 2014. National Oceanic and Atmospheric Administration.
- Hetland, R. D., & DiMarco, S. F. (2008). How does the character of oxygen demand control the structure of hypoxia on the Texas-Louisiana continental shelf? *Journal of Marine Systems*, 70, 49–62. https://doi.org/10.1016/j.jmarsys.2007.03.002
- Hetland, R. D., & DiMarco, S. F. (2012). Skill assessment of a hydrodynamic model of circulation over the Texas–Louisiana continental shelf. *Ocean Modelling*, 43–44, 64–76. https://doi.org/10.1016/j.ocemod.2011.11.009
- Heymans, J. J., Coll, M., Link, J. S., Mackinson, S., Steenbeek, J., Walters, C., & Christensen, V. (2016). Best practice in Ecopath with Ecosim food-web models for ecosystem-based management. *Ecological Modelling*, 331, 173–184. https://doi.org/10.1016/j.ecol-model.2015.12.007
- Kim, H., Franco, A. C., & Sumaila, U. R. (2023). A selected review of impacts of ocean deoxygenation on fish and fisheries. Fishes, 8, Article 316. https://doi.org/10.3390/fishes8060316

- Langseth, B. J., Purcell, K. M., Craig, J. K., Schueller, A. M., Smith, J. W., Shertzer, K. W., Creekmore, S., Rose, K. A., & Fennel, K. (2014). Effect of changes in dissolved oxygen concentrations on the spatial dynamics of the Gulf Menhaden fishery in the northern Gulf of Mexico. Marine and Coastal Fisheries: Dynamics, Management, and Ecosystem Science, 6, 223–234. https://doi.org/10.1080/19425120.2014.949017
- Laurent, A., & Fennel, K. (2014). Simulated reduction of hypoxia in the northern Gulf of Mexico due to phosphorus limitation. *Elementa: Science of the Anthropocene*, 2, Article 000022. https://doi.org/10.12952/journal.elementa.000022
- Laurent, A., Fennel, K., Hu, J., & Hetland, R. (2012). Simulating the effects of phosphorus limitation in the Mississippi and Atchafalaya River plumes. *Biogeosciences*, 9, 4707–4723. https://doi.org/10.5194/bg-9-4707-2012
- Mesinger, F., DiMego, G., Kalnay, E., Mitchell, K., Shafran, P. C., Ebisuzaki, W., Jović, D., Woollen, J., Rogers, E., Berbery, E. H., Ek, M. B., Fan, Y., Grumbine, R., Higgins, W., Li, H., Lin, Y., Manikin, G., Parrish, D., & Shi, W. (2006). North American regional reanalysis. *Bulletin of the American Meteorological Society*, 87, 343–360. https://doi.org/10.1175/BAMS-87-3-343
- Minello, T. J., Able, K. W., Weinstein, M. P., & Hays, C. G. (2003). Salt marshes as nurseries for nekton: Testing hypotheses on density, growth and survival through meta-analysis. *Marine Ecology Progress Series*, 246, 39–59. https://doi.org/10.3354/meps246039
- National Marine Fisheries Service Office of Science and Technology. (2017). Common bottlenose dolphin (Tursiops truncatus truncatus): Northern Gulf of Mexico bay, sound, and estuary stocks. National Oceanic and Atmospheric Administration.
- National Marine Fisheries Service. (2018). Recreational fisheries statistics queries. U.S. Department of Commerce. Retrieved August 22, 2018, from https://www.fisheries.noaa.gov/data-tools/recreational-fisheries-statistics-queries
- Piroddi, C., Akoglu, E., Andonegi, E., Bentley, J. W., Celić, I., Coll, M., Dimarchopoulou, D., Friedland, R., de Mutsert, K., Girardin, R., Garcia-Gorriz, E., Grizzetti, B., Hernvann, P.-Y., Heymans, J. J., Müller-Karulis, B., Libralato, S., Lynam, C. P., Macias, D., Miladinova, S., ... Tsikliras, A. C. (2021). Effects of nutrient management scenarios on marine food webs: A pan-European assessment in support of the marine strategy framework directive. Frontiers in Marine Science, 8, Article 596797. https://doi.org/10.3389/fmars.2021.596797
- Purcell, K. M., Craig, J. K., Nance, J. M., Smith, M. D., & Bennear, L. S. (2017). Fleet behavior is responsive to a large-scale environmental disturbance: Hypoxia effects on the spatial dynamics of the northern Gulf of Mexico shrimp fishery. PLoS One, 12, Article e0183032. https://doi.org/10.1371/journal.pone.0183032
- Rabalais, N. N., Harper, D. E., Jr., & Turner, R. E. (2001). Responses of nekton and demersal and benthic fauna to decreasing oxygen concentrations. In N. N. Rabalais & R. E. Turner (Eds.), Coastal hypoxia: Consequences for living resources and ecosystems (pp. 115–128). American Geophysical Union.
- Rabalais, N. N., & Turner, R. E. (2019). Gulf of Mexico hypoxia: Past, present, and future. Limnology and Oceanography Bulletin, 28, 117–124. https://doi.org/10.1002/lob.10351
- Rozas, L. P., & Minello, T. J. (1997). Estimating densities of small fishes and decapod crustaceans in shallow estuarine habitats: A review of sampling design with focus on gear selection. *Estuaries*, 20, 199–213. https://doi.org/10.2307/1352731
- Sagarese, S. R., Lauretta, M. V., & Walter, J. F. (2017). Progress towards a next-generation fisheries ecosystem model for the northern Gulf of Mexico. *Ecological Modelling*, 345, 75–98. https://doi.org/10.1016/j.ecolmodel.2016.11.001
- Seitzinger, S. P., & Giblin, A. E. (1996). Estimating denitrification in North Atlantic continental shelf sediments. In R. W. Howarth (Ed.), Nitrogen cycling in the North Atlantic Ocean and its watersheds (pp. 235–260). Springer Netherlands.
- Shaffer, M., Marriott, S., Lewis, K. A., Buszowski, J., & de Mutsert, K. (2023). Action science in practice: Co-production of a decision support tool visualizing effects of nutrient and hypoxia reduction goals on fisheries species. Marine and Coastal Fisheries: Dynamics,

- Management, and Ecosystem Science, 15, Article e10262. https://doi.org/10.1002/mcf2.10262
- Shchepetkin, A. F., & McWilliams, J. C. (2005). The Regional Oceanic Modeling System (ROMS): A split-explicit, free-surface, topography-following-coordinate oceanic model. *Ocean Modelling*, 9, 347–404. https://doi.org/10.1016/j.ocemod.2004.08.002
- Smith, M. D., Asche, F., Bennear, L. S., & Oglend, A. (2014). Spatial-dynamics of hypoxia and fisheries: The case of Gulf of Mexico brown shrimp. *Marine Resource Economics*, 29, 111–131. https://doi.org/10.1086/676826
- Smith, M. D., Oglend, A., Kirkpatrick, A. J., Asche, F., Bennear, L. S., Craig, J. K., & Nance, J. M. (2017). Seafood prices reveal impacts of a major ecological disturbance. Proceedings of the National Academy of Sciences of the United States of America, 114, 1512–1517. https:// doi.org/10.1073/pnas.1617948114
- Southeast Data, Assessment, and Review. (2004). SEDAR 5—Complete stock assessment report of Atlantic and Gulf of Mexico King Mackerel.
- Southeast Data, Assessment, and Review. (2010). SEDAR 20—Atlantic Croaker 2010 benchmark stock assessment.
- Southeast Data, Assessment, and Review. (2012). SEDAR 01 update— Stock assessment of Red Porgy off the southeastern United States.
- Southeast Data, Assessment, and Review. (2013a). SEDAR 34—Stock assessment report HMS Atlantic Sharpnose Shark.
- Southeast Data, Assessment, and Review. (2013b). SEDAR 28—Stock assessment report of Gulf of Mexico Spanish Mackerel.
- Southeast Data, Assessment, and Review. (2013c). SEDAR 32A—Stock assessment report of Gulf of Mexico menhaden.
- Southeast Data, Assessment, and Review. (2015). SEDAR 31 update— Stock assessment of Red Snapper in the Gulf of Mexico 1872–2013— With provisional 2014 landings.
- Southeast Data, Assessment, and Review. (2016a). SEDAR 33 update— Stock assessment update report Gulf of Mexico Greater Amberjack (Seriola dumerili).
- Southeast Data, Assessment, and Review. (2016b). SEDAR 49—Stock assessment of Gulf of Mexico data-limited species: Red Drum, Lane Snapper, Wenchman, Yellowmouth Grouper, Speckled Hind, Snowy Grouper, Almaco Jack, Lesser Amberjack.
- Steenbeek, J., Coll, M., Gurney, L., Mélin, F., Hoepffner, N., Buszowski, J., & Christensen, V. (2013). Bridging the gap between ecosystem modeling tools and geographic information systems: Driving a food web model with external spatial-temporal data. *Ecological Modelling*, 263, 139–151. https://doi.org/10.1016/j.ecolmodel. 2013.04.027
- U.S. Environmental Protection Agency. (2025). *Hypoxia Task Force action plans and goal framework*. https://www.epa.gov/ms-htf/hypoxia-task-force-action-plans-and-goal-framework
- Vilas, D., Buszowski, J., Sagarese, S., Steenbeek, J., Siders, Z., & Chagaris, D. (2023). Evaluating red tide effects on the west Florida shelf using a spatiotemporal ecosystem modeling framework. *Scientific Reports*, 13, Article 2541. https://doi.org/10.1038/s41598-023-29327-z
- Walters, C., Christensen, V., Walters, W., & Rose, K. (2010). Representation of multistanza life histories in Ecospace models for spatial organization of ecosystem trophic interaction patterns. Bulletin of Marine Science, 86, 439–459.
- Walters, C. J., & Martell, S. J. D. (2004). Fisheries ecology and management. Princeton University Press.
- Walters, C., Martell, S. J. D., Christensen, V., & Mahmoudi, B. (2008). An Ecosim model for exploring Gulf of Mexico ecosystem management options: Implications of including multistanza life-history models for policy predictions. *Bulletin of Marine Science*, 83, 251–271.
- Yu, H., Fang, G., Rose, K. A., Lin, J., Feng, J., Wang, H., Cao, Q., Tang, Y., & Zhang, T. (2023). Effects of habitat usage on hypoxia avoidance behavior and exposure in reef-dependent marine coastal species. Frontiers in Marine Science, 10, Article 1109523. https://doi.org/10.3389/fmars.2023.1109523
- Yu, L., Fennel, K., Laurent, A., Murrell, M. C., & Lehrter, J. C. (2015). Numerical analysis of the primary processes controlling oxygen dynamics on the Louisiana shelf. *Biogeosciences*, 12, 2063–2076. https://doi.org/10.5194/bg-12-2063-2015